Draft of Jan. 21, 2021

Published as:

Staddon LG, Parkinson IJ, Cavosie AJ, Elliott T, Valley JW, Fournelle J, Kemp AIS, Shirey SB (2021) Detrital chromite from Jack Hills, Western Australia: signatures of metamorphism and constraints on provenance. J. Petrol. 62:12: 30 p. doi: 10.1093/petrology/egab052

Detrital chromite from Jack Hills, Western Australia: signatures of metamorphism and constraints on chromite provenance

Staddon L. G.[1]*¥, Parkinson I. J.[1], Cavosie A. J.[2], Elliott T.[1], Valley J. W.[3], Kemp A. I. S.[4], and Shirey, S. B.[5]

[1]School of Earth Sciences, Wills Memorial Building, Queens Road, University of Bristol, Bristol, UK, BS8 1RJ

[2]School of Earth and Planetary Sciences, Curtin University, Perth, WA 6845, Australia

[3]Department of Geoscience, University of Wisconsin-Madison, Madison, WI 53706, USA

[4]School of Earth Sciences, University of Western Australia, 35 Stirling Highway, Perth 6009, Australia

[5]Earth and Planets Laboratory, Carnegie Institution for Science, Washington DC 20015, USA

*Corresponding author: Leanne.staddon@port.ac.uk

¥Currently at the School of Environment, Geography and Geoscience, Burnaby Building, University of Portsmouth, Burnaby Road, Portsmouth UK, PO1 3QL

KEYWORDS: chromite, Jack Hills, Narryer Terrane, provenance, Archean

ABSTRACT

Detrital chromites are commonly reported within Archean metasedimentary rocks, but have thus far garnered little attention for use within provenance studies. Yet, systematic variations of Cr-Fe spinel mineral chemistry with changing tectonic setting means chromite has been extensively used as a petrogenetic indicator, and so detrital chromites represent good candidates to investigate the petrogenesis of eroded Archean mafic and ultramafic crust. Here, we report the compositions of detrital chromites within fuchsitic (Cr-muscovite rich) metasedimentary rocks from the Jack Hills, geologically renowned for hosting Hadean (>4000 Ma) zircons, situated within the Narryer Terrane, Yilgarn Craton, Western Australia. We highlight signatures of metamorphism, including highly elevated ZnO and MnO, coupled with lowered Mg# in comparison to magmatic chromites, development of pitted domains, and replacement of primary inclusions by phases abundant as metamorphic assemblages within host metasedimentary rocks. Oxygen isotope compositions of detrital chromites indicate partial exchange to complete equilibration with host metasedimentary rocks. Variability of metamorphic signatures between chromites sampled only meters apart further indicates modification occurred *in-situ* by interaction detrital chromites with of metamorphic fluids and secondary mineral assemblages. Alteration likely occurred during upper greenschist to lower amphibolite facies metamorphism and deformation of host metasedimentary rocks at ~2650 Ma. Regardless of metamorphic signatures, sampling location or grain shape, chromite cores yield a consistent range in Cr#. While other key petrogenetic indices, such as Fe_2O_3 and TiO_2 contents, are complicated in Jack Hills chromites by mineral non-stoichiometry and secondary mobility within metasedimentary rocks, we demonstrate that the Cr# of chromite yields significant insights into their provenance. Importantly, moderate Cr# preclude a komatiitic origin for the bulk of chromites. This reflects a dearth of komatiites and associated intrusives within the erosional catchment of the Jack Hills metasedimentary units. We suggest Cr# fit well

with chromites derived from layered intrusions, and that a single layered intrusion may account for the observed chemical compositions of Jack Hills detrital chromites. Thus, we show that, where careful characterisation of key metamorphic signatures is undertaken, detrital chromites may yield valuable information on the petrogenesis and geodynamic setting of poorly preserved mafic and ultramafic crust.

INTRODUCTION

The detrital record of crustal evolution within the early Earth is dominated by analysis of the mineral zircon. This is particularly evident in the Narryer Terrane, within the Yilgarn Craton of Western Australia (Fig. 1). Here, Proterozoic to late Archean (Cavosie *et al.,* 2004; Crowley *et al.,* 2005; Rasmussen *et al.,* 2010; Wang & Wilde, 2018) metasedimentary rocks in the Jack Hills (Fig. 2) yield the oldest known fragments of terrestrial crust; individual grains of detrital zircon yield ^{207}Pb-^{206}Pb ages of up to 4374±6 Ma (Compston & Pidgeon, 1986; Wilde *et al.,* 2001; Valley *et al.,* 2014). Despite isolated occurrences of Hadean detrital zircon elsewhere (*e.g.,* Byerly *et al.,* 2018 and references therein), including Mt. Narryer to the SW (Fig. 1; Froude *et al.,* 1983; Pidgeon & Nemchin, 2006), and rare examples of Hadean xenocrystic zircon (Nelson *et al.,* 2000; Wyche *et al.,* 2004; Iizuka *et al.,* 2006; Chaudhuri *et al.,* 2018), Jack Hills detrital zircons represent critically important remnants of Hadean (>4000 Ma) crust.

These zircons therefore provide a unique window into the Hadean Earth, and have subsequently been rigorously interrogated using numerous geochemical and isotopic techniques (*e.g.,* Cavosie *et al.,* 2018). Previous investigations have broached a wide range of subjects, including Earth's ancient dynamo (Borlina *et al.,* 2020; Tarduno *et al.,* 2020), the origins of life (Bell *et al.,* 2015) and the role of impacts within the early Earth (Bell & Harrison, 2013; Cox *et al.,* 2017). Despite intense study, what Jack Hills zircons tell us about the composition, evolution and subsequent destruction of their original host rocks is controversial, with conflicting hypotheses inferring vastly disparate geodynamic conditions within the early Earth. Such hypotheses include a 'cool early Earth' (*e.g.,* Valley *et al.,* 2002), with the putative operation of plate tectonics (Harrison *et al.,* 2008; 2017; Bell *et al.,* 2014), production of zircon-bearing crust by internal reworking of mafic protocrust (Amelin *et al.,* 1999; Kemp *et al.,* 2010), or compositionally diverse Hadean protoliths (Wang & Wilde, 2018).

While the Jack Hills zircon record yields valuable, if controversial, constraints on the evolution of felsic Hadean and Archean crust, the zircon record provides little information on the evolution of contemporaneous mafic and ultramafic crust. This is of particular importance, as emerging evidence suggests mafic to ultramafic crust was the dominant compositional component of the Archean (*e.g.,* Dhuime *et al.,* 2015; Kamber *et al.,* 2015; Tang *et al.,* 2016). Evolved, zircon-bearing crust may therefore be over represented within detrital records, in part due to the poorer preservation potential of its mafic to ultramafic counterparts. While the wider Yilgarn Craton is renowned for the presence of economically significant komatiites (Arndt *et al.,* 2008), the generation and evolution of mafic and ultramafic crust within the Narryer Terrane is poorly constrained. Indeed, the only >3100 Ma mafic and ultramafic crust described within the entire Yilgarn Craton is the Eoarchean Manfred Complex (Wyche, 2007), a 3730 Ma disseminated layered intrusion within the Narryer Terrane (Fletcher *et al.,* 1988; Kinny *et al.,* 1988; Myers, 1988b; Rowe & Kemp, 2020).

However, the largely unexplored eroded remnants of mafic and ultramafic crust are ubiquitous within Jack Hills metasedimentary rocks, in the form of detrital chromite. Unlike zircon and other detrital phases observed at Jack Hills, including minor monazite and xenotime (Rasmussen *et al.,* 2010; Iizuka *et al.,* 2010), chromite has a magmatic provenance restricted solely to mafic and ultramafic crust (Barnes & Roeder, 2001). Furthermore, chromites within their mafic or ultramafic protoliths are frequently used as a petrogenetic indicator, owing to the presence of systematic chemical variations in chromite formed under different tectonic conditions (Irvine, 1965; 1967; Dick & Bullen., 1984; Roeder, 1994; Barnes & Roeder, 2001; Kamenetsky *et al.,* 2001). Critically, the sequestration of platinum group elements (PGEs) into spinel means that chromite is amenable to geochronology using Re-Os and Pt-Os decay systems (Shirey & Walker, 1998), potentially allowing a temporal framework of the generation of chromite-bearing mafic and ultramafic crust to be constrained from the detrital record. The

value of detrital chromites for elucidating the provenance of magmatic protoliths has previously been demonstrated (*e.g.,* Barnes & Roeder, 2001; Lenaz & Princivalle, 2005; Barkov *et al.,* 2013), though additional care is required to quantify the effects of metamorphism on detrital chromite found within ancient terranes (Barnes, 2000; Colás *et al.,* 2014). Understanding how and when the Jack Hills detrital chromite formed will therefore provide valuable information on the composition and petrogenesis of poorly described mafic and ultramafic crust that was potentially exposed at the time the Jack Hills sedimentary succession was deposited

Here, we report major and minor element geochemistry of detrital chromites from thirteen samples of metasedimentary rocks collected from within the Jack Hills (Fig. 2). This study combines data collected by two groups (University of Bristol; 14WA and 16WA samples and University of Wisconsin-Madison; 01JH samples), representing the first systematic study of detrital chromite from Archean sedimentary rocks, and signifying a new direction compared to traditional provenance studies undertaken by analysis of detrital zircon. We highlight the effects of metamorphism on chromite mineral chemistry, discuss the retention of primary signatures, and propose a plausible provenance for detrital chromites. Finally, we discuss the significance of these grains for enhancing our understanding of the metamorphic history of the Jack Hills metasedimentary rocks, the distribution of mafic and ultramafic crust within the Archean upper crust at the time of deposition, and the wider potential of detrital chromites for provenance studies of ancient mafic and ultramafic crust.

GEOLOGICAL SETTING

The Narryer Terrane

The Narryer Terrane is the most north-westerly terrane within the Yilgarn Craton, in Western Australia (Myers, 1988a; Kemp *et al.,* 2018; Fig. 1), and has been interpreted as a deep crustal

allochthon thrust above the Youanmi Terrane (Nutman *et al.,* 1993), prior to or coincident with cratonic amalgamation (Kemp *et al.,* 2018). The terrane is dominantly composed of granitic lithologies, now largely preserved as quartzofeldspathic orthogneisses with >3 Ga protolith ages, with minor ultramafic and mafic intrusives, and metasedimentary rocks (Myers & Williams, 1985; Williams & Myers, 1987; Myers, 1988a). Neoarchean (~2700-2650 Ma) granitic rocks are also abundant (Kemp *et al.,* 2018). Much of the Narryer Terrane has undergone high-grade, polyphase deformation, with amphibolite to granulite facies events at ~2700-2650 Ma forming the observed gneissic fabric (Myers, 1988a; Kinny, 1990; Nutman *et al.,* 1991). There is evidence for previous high-grade thermal events, particularly at ca. 3300 Ma (Nutman *et al.,* 1991; Kinny & Nutman, 1996), and it has been postulated orthogneisses within the Narryer Terrane underwent multiple episodes of deformation and anatexis during the Archean (Kinny & Nutman, 1996).

Despite complicated zircon geochronology (Pidgeon & Wilde, 1998), three dominant quartzofeldspathic orthogneiss units are identified within the Narryer Terrane (Kemp *et al.,* 2018). The Meeberrie gneiss is a biotite-rich migmatite that consists of 3670-3600 Ma monzogranitic and 3730 Ma tonalitic protoliths (Nutman *et al.,* 1991; Kinny & Nutman, 1996; Pidgeon & Wilde, 1998). The Eurada gneiss is a series of ~3480 Ma tonalitic gneisses that comprise a fault bound lozenge west of Mount Narryer (Nutman *et al.,* 1991). The Dugel gneiss yields a well constrained age of 3375±26 Ma (Nutman *et al.,* 1991) and it is thought that its syenogranitic protoliths intruded the Meeberrie Gneiss as a series of sheet-like and pegmatitic bodies (Myers, 1988a; Kemp *et al.,* 2018).

The Meeberrie and Dugel gneiss host dispersed fragments of the Manfred Complex, a magmatically and tectonically dismembered and variably metamorphosed layered intrusion. The complex is dominantly amphibolitic (after gabbro and leucogabbro), with pyroxenite, metaperidotite and anorthosite (Williams & Myers, 1987; Fletcher *et al.,* 1988; Myers, 1988b;

Rowe & Kemp, 2020). Relict igneous textures and layering are locally preserved (Kemp *et al.,* 2018). Zircon within Manfred Complex anorthosite and leucogabbro yield $^{207}Pb/^{206}Pb$ ages of 3730±6 Ma (Kinny *et al.,* 1988; Kemp *et al.,* 2018), with other lithologies yielding Sm-Nd and Pb-Pb whole rock (WR) ages of 3680±70 Ma and 3689±146 Ma, respectively (Fletcher *et al.,* 1988). Spinel (spinel *sensu-stricto* to picotite) and olivine chemical compositions are consistent with formation of the Manfred Complex within a thickened oceanic plateau; reduced, high Al-Ca-Fe picritic to tholeiitic basaltic parental melt compositions are thought to be derived from shallow partial melting of spinel lherzolite (Rowe & Kemp, 2020).

Jack Hills

The Jack Hills are located at the southern margin of Narryer Terrane (Figs. 1 & 2) and comprise a thin, ~70km-long belt, with a distinctly curvilinear morphology produced by dextral shearing (Spaggiari, 2007a). The Jack Hills belt is tectonically juxtaposed with the surrounding gneisses, except for localised intrusion of 2654 Ma monzogranite, also known as 'The Blob' (Pidgeon & Wilde, 1998; Spaggiari *et al.,* 2007b), and has been interchangeably referred to as a greenstone (*e.g.,* Spaggiari *et al.,* 2007a/b) or metasedimentary/supracrustal belt (*e.g.,* Wang & Wilde, 2018). It largely consists of siliciclastic units, including metaconglomerate, quartzite and quartz-mica schist, with minor intercalated mafic and ultramafic rocks, banded iron formation (BIF) and chert. The presence of grunerite within BIF and hornblende within mafic schist indicates at least portions of the belt have reached amphibolite facies metamorphism; later greenschist facies metamorphism defines the dominant metamorphic signature of the belt (Spaggiari, 2007a).

Deformation has tectonically disturbed and juxtaposed lithological associations, making an original stratigraphy difficult to discern. Spaggiari (2007a) divided the belt into four associations determined by lithological variability (Fig. 2). Briefly, association 1 consists of

interbedded BIF, chert and quartzite, mafic and ultramafic rocks, and black and white banded quartzites. Association 2 yields pelitic to semi-pelitic associations, now present as quartz-mica and andalusite schists, with accompanying mafic schist and quartzite. The presence of an S1 cleavage and recumbent folding absent from other lithological units suggests associations 1 and 2 were deformed prior to the deposition of units 3 and 4 (Spaggiari, 2007a). Association 3 is restricted to the central region of the belt at Eranondoo Hill (Fig. 2), and was derived from mature, siliciclastic sediments interpreted to have been deposited within a deltaic alluvial fan (Spaggiari *et al.,* 2007a/b) between ~3050 Ma and 2650 Ma (Crowley *et al.,* 2005; Rasmussen *et al.,* 2010). The discovery of Proterozoic detrital zircons (Cavosie *et al.,* 2004; Dunn *et al.,* 2005; Grange et al., 2010) within the Jack Hills belt led to the recognition of Unit 4, which hosts metasedimentary rocks deposited during the Proterozoic. Wang & Wilde (2018) observed interbedded siliciclastic units at the same apparent metamorphic grade but with both Archean and Proterozoic depositional ages, highlighting that the depositional and/or tectonic relationships of units 3 and 4 may be more complex than previously postulated.

Metasedimentary rocks within Jack Hills show clear indications of deformation; intense shearing is particularly evident within the anastomosing micaceous matrix, where a strong foliation is coincident with flattening and recrystallisation of quartzite cobbles (Spaggiari, 2007a). Thermal or fluid events within the Jack Hills belt occurred at ~3080 Ma, 2650 Ma, ~1850-1800 Ma and 800 Ma (Spaggiari, *et al.,* 2007b; Rasmussen *et al.,* 2010; 2011). Monazite-xenotime thermometry of secondary inclusions within detrital zircon yield temperatures of 420-475 °C (Rasmussen *et al.,* 2011), argued to represent peak upper greenschist to lower amphibolite facies metamorphism within unit 3 metasedimentary rocks at ~2650 Ma (Rasmussen *et al.,* 2010). However, like the depositional ages of metasedimentary units, the exact P-T conditions and timing of metamorphism within unit 3 and 4 metasedimentary units are ambiguous (Kemp *et al.,* 2018). A Proterozoic overprint at ~1800 Ma (Spaggiari *et al.,*

2007b; Rasmussen *et al.,* 2010) and a discrete event at 800 Ma (Rasmussen *et al.,* 2010; 2011) are of unknown metamorphic grade, but also coincide with formation of monazite and xenotime (Rasmussen *et al.,* 2010; 2011).

Metasedimentary rocks from Eranondoo Hill, chiefly oligomict pebble to cobble metaconglomerate and quartzite, are renowned for hosting Hadean detrital zircon (Compston & Pidgeon, 1986; Wilde *et al.,* 2001), with most studies focused on metasedimentary rocks at the W-74 'discovery site' (Fig. 2). Unsurprisingly, Jack Hills detrital zircons have been the subject of numerous publications and reviews (*e.g.,* Harrison *et al.,* 2017; Cavosie *et al.,* 2018). While a detailed description of the zircons is beyond the remit of this publication, it is important to note there is some debate surrounding the source of detrital zircon ^{207}Pb-^{206}Pb age distribution peaks, and thus the source of detritus. Whilst ^{207}Pb-^{206}Pb age peaks correspond with major units of the Narryer Terrane and the granitic lithologies surrounding Jack Hills (Nutman *et al.,* 1991; Pidgeon & Wilde, 1998), distal sources of more intermediate composition have also been suggested (Crowley *et al.,* 2005). Additionally, the protoliths of >3800 Ma zircons are unknown, and may derive from a source exogenous to the Narryer Terrane. Sources external to the Narryer Terrane therefore cannot be discounted for detrital chromites. If detrital phases are derived from the Narryer Terrane, a further consideration is that both detrital zircon and chromite are present within quartzite clasts of the metaconglomerates (*e.g.,* Grange *et al.,* 2010; Dare *et al.,* 2016). This demonstrates that the detrital phases have undergone multiple sedimentary cycling events. It is therefore plausible that the source of detrital chromite had already been completely or partially eroded at the time of deposition of the Jack Hills sediments (3050 Ma to 2650 Ma), and therefore may not represent the distribution of mafic and ultramafic crust during the late Archean (Crowley *et al.,* 2005; Rasmussen *et al.,* 2010).

Despite concerted interest in detrital zircon at Jack Hills, detrital chromites within the same metasedimentary rocks have garnered less attention. Detrital chromites with low Mg#

(100x molar Mg/(Mg+Fe^{2+})) and elevated ZnO and MnO were reported by Cavosie *et al.* (2002) for grains from the W-74 site; comparable major element compositions were described by Dare *et al.* (2016) in analyses of detrital chromites ~1 km to the NW of this locality. Dare *et al.* (2016) proposed that low MgO contents of chromites precluded derivation of Jack Hills detrital chromites from komatiites, and that both chromite and Fe-Ni-sulphides observed within quartzite clasts are the erosional products of at least one layered intrusion. Unpublished Re-Os model ages (T_{MAs}) of 3500 Ma to 3200 Ma were reported by Valley *et al.* (2005) for the same population of chromites described within Cavosie *et al.* (2002). These data suggest the analysed detrital chromites are at least Palaeoarchean in age, and highlight the potential preservation of robust Re-Os systematics through peak metamorphism within the Jack Hills.

METHODS AND MATERIALS

Sample collection and preparation

Sampling locations of metasedimentary rocks are shown in Fig. 2. Seven samples of pebble metaconglomerates (14WA1-4, 16WA5-6 and 01JH54) were collected from within 10 m of the W-74 site (Wilde *et al.,* 2001) at Jack Hills (Fig. 2b). A further sample of pebble metaconglomerate (16WA8) and a quartzite (16WA7) were collected along strike approximately 35m to the WSW. Two pebble metaconglomerates (16WA9-10) were sampled from a prominent ridge across the valley to the NE. 01JH35 is a metaconglomerate sampled ~800 m to the NE of the W-74 site. 01JH36, collected approximately 200m to the ENE of 01JH35, is a quartzite with discrete, mm-scale heavy mineral bands (Cavosie *et al.,* 2004). Petrographic sample descriptions of metasedimentary rocks and their detrital mineral assemblages are provided in supplementary material. While fuchsite-rich (muscovite with >1 wt. % Cr_2O_3; Challis *et al.,* 1995) metasedimentary rocks were largely collected to yield the

highest concentrations of chromite grains, 01JH36, 16WA6 and 16WA10 lack significant fuchsite. Two chromite-bearing ultramafic rocks from within the Narryer Terrane are also included, with descriptions and sampling locations provided within Supplementary Material. Sample 13TKN22 is a metaperidotite from the 3730 Ma Manfred Complex, collected from NE of Mt. Narryer, ~60 km SW of the Jack Hills. Sample 16WA13 is a heavily recrystallised ultramafic rock of unknown age sampled from the SW limb of Jack Hills (Fig. 2a); this sample is part of association 1 of Spaggiari *et al.* (2007a) and so is considered >3000 Ma.

Chips of Narryer Terrane ultramafic rocks were mounted in epoxy for petrographic study and identification of chromite. 14WA, 16WA and 01JH35 chromites were separated using standard crushing and separation procedures, then sieved to yield size fractions of ≤500 μm for analysis. 01JH36 and 01JH54 chromites were separated by electric pulse disaggregation (EPD). 14WA1-4 heavy minerals were concentrated using the Wilfey table, followed by magnetic and heavy liquid separation, while 16WA5-10 separates were concentrated via panning. 01JH chromites were concentrated using heavy liquids and magnetic separation. Chromites were picked by hand, separated per sample location, grain size and rounding shape, and mounted in epoxy. Detrital grains within a thin section of 14WA2 were also analysed, as were chromite liberated via HF leaching of quartzite cobbles from 14WA2 and 16WA5. No chemical differences between chromites present within quartzite cobbles or matrix were observed, so they are discussed together below.

Chromite mineral chemistry

14WA, 16WA and 13TKN22

Chromites were imaged using reflected light microscopy and/or back scattered electron imaging using a Hitatchi S-3500N scanning electron microscope at the University of Bristol. Chromite major elements were determined from individual spots and line scans using the Cameca SX100

electron microprobe at the University of Bristol. Chromium, Al, Fe, Mg, Zn, Mn, Ti, V, and Ni abundances of chromite were determined using a 20kV accelerating voltage, a 10nA beam current, 1 μm beam diameter, and a PAP matrix correction. Silicon, Na and Ca were included within the set up to monitor any silicate contamination; analyses with >0.15 wt.% oxide of these elements were omitted. Counting times were 30s for Cr, Fe, Al and Zn and 60s for Ti, Ca, Mg, Na, Mn, V, Si and Ni, with the following standards used for instrument calibration: Cr_2O_3 (Cr), albite (Al and Na), ilmenite (Fe and Ti), St. John's olivine (Mg and Si), Zn metal (Zn), Mn metal (Mn), V metal (V), Ni metal (Ni) and wollastonite (Ca). The overlap of Ti Kβ on V Kα was corrected either via analysis of V-free $SrTiO_3$, or using high-resolution slits. No resolvable variability in the V_2O_3 contents of chromite or chromite secondary standards was observed between the two set-ups. Typical detection limits, expressed in ppm, were: Cr(260), Al(250), Na(450), Fe(320), Ti(120), Mg(250), Si(180), Zn(400-500), Mn(300), V(200), Ni(350) and Ca(140).

Four spinel standards (8316, 8311, 79-1 and 8315), well characterised for $Fe^{3+}/\Sigma Fe$ using both EPMA and Mössbauer from Wood & Virgo (1991), were analysed *in-run* to monitor the integrity of EPMA measurements. Long term reproducibility of major elements (Al, Cr, Fe, Mg) within 8316 and 8311, which possess the most comparable mineral chemistry to samples, are <1.2 wt.% (2σ). The method of Droop (1987) was employed to calculate the ferric iron content of chromite by stoichiometry. The determined $Fe^{3+}/\Sigma Fe$ (molar 100x $Fe^{3+}/(Fe^{3+}+Fe^{2+})$) of 8316 (0.21±0.07; 2σ) and 8311 (0.17±0.06; 2σ), measured across multiple analytical sessions, are in good agreement with reported values. After correction for ferric iron, 14WA4, 16WA6 and 16WA9-10 yielded chromite with systematically low totals, typically between 97% and 98%, despite other analyses within the same run yielding good totals. The cause of low totals within these samples is unknown but may reflect non-stoichiometry, likely due to site vacancies. Fe_2O_3 contents of chromite should therefore be considered minimum abundances for

14WA and 16WA samples. Chromites with totals of 97.5-102% from 14WA4, 16WA6 and 16WA9-10 are included, while measurements from other samples are restricted to those that yield totals of 98-102%.

01JH samples

EPMA analyses were undertaken at the University of Wisconsin-Madison Department of Geoscience using a CAMECA SX51 electron microprobe equipped with Probe for EPMA software. Analyses were conducted at 20 kV, with a 20 nA beam current and a focused electron beam. Count times for all elements were 10 seconds on peak and a total of 10 seconds on off-peak background positions. The matrix correction was the PAP procedure. PHA differential was used for Al and O, other elements were in integral mode. Oxygen was determined with a 60° 2d PC0 diffractor crystal, while Si, Al and Mg were acquired on TAP, Ti and Cr on PET, and V, Mn, Fe, Ni, Cu and Zn on LIF. Overlap corrections were made on Al for Cr, Ni and Ti, on V for Ti, on Fe for Mn, and on O for Cr. The following standards were used for instrument calibration: USNM Chromite (Cr, Al, Mg, O), Harvard University hematite (Fe), synthetic tephroite (Mn, Si), V_2O_5 (V), rutile (Ti), Ni_2SiO_4 (Ni), $ZnAl_2O_4$ (Zn) and Cu_2O (Cu). Reproducibility, Detection limits.

EPMA analyses were processed using two methods. In the first, oxygen measurements were omitted and analyses were processed using the same techniques as 14WA and 16WA; namely, calculation of ferric iron by stoichiometry using the method of Droop (1987), and exclusion of analyses with >0.15 wt.% SiO_2 and totals of <98 %. In the second method, cations and measured oxygen were converted into molar proportions, and the ferrous/ferric ratio of iron adjusted to balance the negative charge from measured O. This technique assumes Fe is the only multivalent cation present (*e.g.,* Cr is present as Cr^{3+}, V as V^{3+} and Mn as Mn^{2+}) and that site vacancies are negligible. The latter scenario is unlikely to be true within altered Cr-rich

spinel (see Kamperman *et al.,* 1996), and so ferric iron compositions determined by the second method represent maximum values. For consistency, data calculated using stoichiometry are presented within the main text, while analyses processed using measured O are discussed in supplementary material.

Oxygen isotope analyses

Chromite grains from samples 01JH36, 01JH42 and 01JH54 were analysed for oxygen isotope ratio by laser fluorination at the University of Wisconsin-Madison Department of Geoscience. A total of 35 analyses of oxygen isotope ratio in chromite were made using gas source mass spectrometry with BrF_5 and a 32 W CO_2 laser (Valley *et al.,* 1995). Chromite data were corrected for accuracy with the UWG-2 garnet oxygen standard, which was analysed multiple times at the beginning of the session (Valley *et al.,* 1995). The reproducibility of UWG-2 per session ranged from ± 0.06 to ± 0.24 (2σ). Samples of chromite were first sieved into seven size fractions, ranging from 105-149 μm to >500 μm (Supplementary Table 1). At least three size fractions were analysed from each sample, with two to three aliquots analysed of each size fraction. Aliquots of chromite were prepared by soaking detrital grains in concentrated HF at room temperature overnight. Each ~2 mg aliquot of chromite thus consisted of hundreds of clean detrital grains. Values are reported in standard per mil notation relative to V-SMOW (Vienna Standard Mean Ocean Water).

RESULTS

Chromite morphology and inclusion assemblages

Jack Hills detrital chromites are ≤500 μm grains of variable morphology that are enclosed by, or closely associated with, fuchsite within quartzite or metaconglomerate matrix (Fig. 3a). Finer

(≤100 μm) chromite grains have previously been reported within metaconglomerate quartzite cobbles (Dare *et al.,* 2016), but were uncommon in samples of this study (Fig. 3b), though HF leaching of quartzite cobbles liberated a small number of grains (n= 12). Many chromites show textural evidence of sedimentary transport, including abrasion and rounding of broken surfaces. Chromite derived from Jack Hills metasedimentary rocks occur as euhedral octahedra (EO), rounded octahedra (RO) or rounded grains (RC: rounded chromite) (Fig. 3a). EO yield minimal rounding on two or fewer faces, with many euhedral grains showing little or no evidence of sedimentary transport. RC grains demonstrate limited evidence of original habit on two or less faces, and are often present as highly spherical morphologies. RO are chromites with morphologies intermediate to EO and RC, and are the most abundant morphology. More quartzitic lithologies possess a greater proportion of euhedral grains. 16WA9 and 16WA10, sampled furthest from the W-74 site, yield a more bimodal distribution with chromite dominantly RC and minor EO.

A range of internal textures are present (Fig. 4), with grains often heavily cracked and displaying ragged or lobate boundaries with surrounding fuchsite (Fig. 3c). Fractures occasionally display distinct polygonal morphologies (Fig. 4b), and larger fractures may be filled with quartz, fuchsite, and Fe-oxide. Distinct 'pitted' textural domains within chromite reveal the presence of typically ≤10 μm inclusions of dominantly quartz and fuchsite (Figs. 4&5). Rare porous textures with ≥30 μm inclusion assemblages may occasionally account for the majority of the grain (Fig. 4e-f). Both pitted and porous domains are conspicuous at chromite rims or adjacent to cracks, and particularly where chromite is enclosed by fuchsite. Fine laths of rutile, often showing apparent alignment to chromite crystallographic directions, are also commonly associated with pitted and porous domains (Fig. 4e-f & 5a). Isolated monomineralic and polyphase silicate and oxide inclusions present within chromites are typically globular or anhedral in habit (Fig. 5), but may more rarely possess subhedral to

385 euhedral morphologies (Fig. 5a&d). Inclusions associated with fractures and crack filling
386 assemblages of quartz, fuchsite and rutile (Fig. 5a-b&e) are often accompanied by other fine-
387 grained (typically ≤10 μm) phases, including Fe-oxide (Fig. 5b), Fe-sulphide (Fig. 5c), and
388 rarer monazite (Fig. 5f).
389
390 Chromite mineral chemistry
391 Representative analyses of detrital chromites from each metasedimentary sample location are
392 presented in Table 1, and the full EPMA data set is available in Supplementary Material 2.
393 Chromite major element abundances show no variation with grain size or rounding shape
394 (Supplementary Figs.) but differ systematically between sampling locations (Figs. 6 & 7).
395
396 *Sample variability (Ti^{4+} and divalent cations; Fe^{2+}, Mg^{2+}, Zn^{2+}, Mn^{2+}, and Ni^{2+})*
397 Chromite from all sampled metasedimentary rocks yield elevated ZnO (up to 13 wt.%) and
398 MnO (up to 4.4 wt.%), coupled with low Mg# (typically ≤30; Fig. 6). Largely, samples with
399 increasingly elevated ZnO yield lower and more homogeneous Mg# (Fig. 6a). 14WA2
400 chromites possess the lowest wt.% ZnO (average ZnO 1.23 wt.%) and largest range of Mg#,
401 with a single grain (14WA2-PB-46) yielding Mg# of ~30. Unusually elevated MnO contents
402 are present in 01JH35, where chromites yield >3.5 wt.% MnO (Fig. 6b). No variation of MnO
403 with Mg# is apparent (Fig. 6b), though some 16WA samples show variance between ZnO and
404 MnO (Fig. 6d).
405 TiO_2 is typically <1 wt.% (Figs. 6c). Individual analyses where TiO_2 is above 1 wt.%
406 correlate with areas where laths of rutile are present, and are omitted from consideration.
407 Elevated TiO_2 of ≥1 wt.% is most apparent within lower Cr# (100x molar Cr/(Cr+Al)) grains
408 (Fig. 7). As the bulk of analyses possess ≤0.3 wt.% TiO_2, this suggests analyses yielding TiO_2
409 >0.3 wt.% may also overlap with rutile laths. However, many chromites with ~0.3-0.8 wt.%

TiO_2 show no evidence of rutile laths in BSE images. NiO within grains is largely below the quantification limit of ~0.04 wt.%.

Sample variability (trivalent cations: Cr^{3+}, Al^{3+}, V^{3+}, Fe^{3+})

Despite considerable variability of divalent cation contents between sampling locations, detrital chromite show a similar range in Cr# between samples (Fig. 7). Chromites yield moderate to high, and variable Cr# of 48-82, with the bulk of chromites displaying Cr# of 54-66 (Fig. 7a). The apparent smaller range of Cr# in chromites with higher wt.% ZnO is likely a sampling bias due to fewer analyses. V_2O_3 was not measured for 16WA5-7, but where measured is present at 0.05 wt.%, to 0.37 wt.% and shows no inter-sample variability. Jack Hills detrital chromites yield low calculated Fe_2O_3 contents; the bulk of the population contain ≤2 wt.% Fe_2O_3, though analyses with up to 8 wt.% Fe_2O_3 are present. This results in highly variable $Fe^{3+}/\Sigma Fe$ (100x molar $Fe^{3+}/(Fe^{3+}+Fe^{2+})$) ratios of 0-20 (Fig. 7d). Many chromites yield non-stoichiometric compositions (*e.g.,* deviation from $A^{2+}B^{3+}{}_2O_4$), shown by cation totals of less than 3 when normalised to 4 oxygens. This likely reflects cation vacancies (*e.g.,* Kamperman *et al.,* 1996), and results in an under-estimation of ferric iron contents by stoichiometric calculations (Droop, 1987). Non-stoichiometry also affects analyses conducted by direct measurement of oxygen (Supplementary Material); analyses with significant cation deficiency results in substantial over-estimation (>10 wt. %; Supplementary Material) of ferric iron contents to balance the negative charge of oxygen. Thus, stoichiometric and charge balance of 01JH analyses represent minimum and maximum ferric iron contents of Jack Hills detrital chromites, respectively.

Within grain variability

Zoning; While the largest systematic variations in chromite chemistry are between sample location, line scans of 14WA and 16WA detrital chromites reveal distinct zonation trends (Fig.

8). Chromites do not exhibit morphologically or microstructurally distinct cores and rims, but we use those terms here to describe the centre and outer portions of grains. Most chromites have homogeneous ZnO contents (Fig. 8a) or else slightly lower wt.% ZnO towards rims (Fig. 8b-c). MnO is largely uniform across chromites, although slightly lower abundances towards the rim may be observed. Homogeneous Mg# appears to be restricted to chromites within high ZnO 16WA7 (Fig. 8c), with all other samples yielding chromites that display distinct variability in Mg#. Low ZnO samples, such as 14WA2 and 16WA5, yield clear decreases in Mg# from the core to rim of the grain (Fig. 8a). High ZnO samples, such as 14WA3 and many examples within 14WA4, often yield rims with higher Mg# (Fig. 8b) though lowering of Mg# from core to rim is also observed. Grains with elevated Mg# at the rims show increases in both MgO and FeO from core to rim, compensated by decreases in ZnO and MnO.

While grains yield zoning profiles of divalent cations, intra-grain changes in Cr# are largely absent (Fig. 8). Core-to-rim trends of marginally higher or lower Cr# (*e.g.,* ±2) are sometimes observed (Fig. 8 a&c), but there is no systematic behaviour in samples from different locations. Like Cr#, Fe_2O_3 contents are generally homogeneous across chromite grains, with variability in some zonation profiles likely reflecting low calculated Fe_2O_3 contents. However, individual grains do yield distinct variations in Fe_2O_3 that appear systematic in origin, present as both decreases and enrichments in Fe_2O_3 from core to rim, with increasing Fe_2O_3 often coupled with a small increase in Cr# (Fig. 8a).

Coupled elemental and textural variation; Distinct zones of elevated Cr# within detrital chromite are rarely present (Fig. 9). These features are closely associated with pitted domains and fractures, and exhibit both diffuse and more commonly sharp (Fig. 9a-e) boundaries with surrounding chromite. High Cr# domains, often distinguished by an absence of fractures and inclusions in comparison to surrounding chromite (Fig. 9a-b), mostly occur at the edge of grains

460 adjacent to enclosing fuchsite or associated with fractures (Fig. 9a-c). These domains may also
461 be localised, occurring as distinct polygonal areas defined by crystallographic directions (Fig.
462 9d-e). These domains are characterised by high Cr# (>70), low totals (<98 wt.%), the apparent
463 absence of Fe_2O_3, lower ZnO and V_2O_3, and occasionally slightly elevated MnO. High Cr#
464 domains within detrital chromite are chemically indistinguishable from low Fe_2O_3, high Cr#
465 grains within the same samples. Only a single domain of low Cr# has been observed within
466 chromite, bounding a monomineralic quartz inclusion alongside iron oxide (Fig. 9f).
467
468 Oxygen Isotope Compositions
469 Analysis of oxygen isotope ratio in various chromite size fractions was conducted to determine
470 if detrital chromite grains preserve primary (magmatic) $\delta^{18}O$ values, or if there is evidence of
471 oxygen exchange with the metasedimentary host rocks. Exchange of oxygen isotopes between
472 chromite and surrounding quartz at low temperature (*e.g.,* <600 °C) would result in lowered
473 $\delta^{18}O$ values for chromite (*e.g.,* Lowry *et al.,* 2003). Each sample showed >1 ‰ variability in
474 $\delta^{18}O$, with $\delta^{18}O$ chromite values ranging from 0.03 to 2.19 ‰ (Fig. 10; Supplementary Table
475 1). For samples 01JH36 and 01JH42, the lowest chromite $\delta^{18}O$ values (0.69 and 0.03 ‰,
476 respectively) were detected in the smallest size fraction, and there was a systematic increase of
477 $\delta^{18}O$ with grain size (Fig. 10a-b). In contrast, 01JH54 showed no systematic variation of
478 chromite $\delta^{18}O$ with grain size, and also contained the highest $\delta^{18}O$ measured for chromite at
479 2.19 ‰ (Fig. 10; Supplementary Table 1).
480
481
482 DISCUSSION
483
484 Chromite morphology and the origin of inclusion assemblages

485 The variably rounded morphologies of chromite, from RC to EO, attests to a protracted and
486 complex reworking history of numerous detrital grains. Further to this, the presence of chromite
487 within quartzite cobbles of metaconglomerates (Fig. 3b; Dare *et al.,* 2016) suggests cycling of
488 some grains in at least two sedimentation events. Categorisation of grains by shape may indicate
489 provenance from multiple geographic sources or differing modes of sedimentary transport
490 (Dott, 2003). The extensive sedimentary cycling history of some chromites is consistent with
491 the mature nature of host metasedimentary rocks (>98 wt.% SiO_2; Cavosie et al., 2004), but at
492 odds with the highly fractured nature of many grains (Fig. 4b-e), which would not survive
493 extensive sedimentary transport. This strongly suggests that fracturing of grains occurred *in-*
494 *situ*, likely alongside deformation of the host metasedimentary rocks.
495 Jack Hills detrital chromites contain inclusion assemblages of quartz, fuchsite, rutile,
496 Fe-oxide, monazite, and Fe-sulphide (Fig. 5). These phases, particularly silicates quartz and
497 fuchsite, typically form under distinctly different conditions to magmatic chromite. However,
498 quartz and fuchsite are common components of Jack Hills quartzites and metaconglomerates,
499 alongside minor secondary rutile, monazite and xenotime (Harrison *et al.,* 2007; Rasmussen *et*
500 *al.,* 2010; Iizuka *et al.,* 2010). Inclusions of quartz and Cr-poor muscovite have also been
501 reported within detrital zircon (Cavosie *et al.,* 2004; Hopkins *et al.,* 2008; 2010; Rasmussen *et*
502 *al.,* 2011; Bell *et al.,* 2015), both as monomineralic and polyphase inclusions alongside
503 monazite and xenotime (Rasmussen *et al.,* 2011). Monazite and xenotime inclusions within
504 detrital zircons yield ^{207}Pb-^{206}Pb ages of ~2650 Ma and 800 Ma that are demonstrably younger
505 than the host grains (Rasmussen *et al.,* 2011), attesting to a secondary origin of many zircon
506 inclusion assemblages. Cameron *et al.* (2016) additionally showed that ~60 % of quartz
507 inclusions within zircon exhibited evidence of $\delta^{18}O$ exchange with Jack Hills metasedimentary
508 rocks. It is therefore hypothesised that many quartz inclusions within detrital zircons were
509 significantly altered during metamorphism of host metasedimentary rocks or, alongside

muscovite, rutile, monazite and xenotime, were precipitated from post-depositional fluids that filled voids left from the dissolution of primary apatite (Rasmussen *et al.,* 2012; Bell *et al.,* 2015; Cavosie *et al.,* 2018; *c.f.* Hopkins *et al.,* 2010; 2012).

The occurrence of assemblages of the same phases as observed within detrital zircon, coupled with the unlikelihood of quartz and muscovite stability within the mafic-ultramafic melt that crystallised chromite, provides evidence that inclusion assemblages within chromite are secondary in origin. Interestingly, many secondary inclusions of quartz and fuchsite are apparently isolated from visible fractures within chromites (*e.g.,* Fig. 5a & 8a). Isolation of inclusions has been used as a line of evidence for a primary origin of many quartz and muscovite inclusions within detrital zircon (Bell *et al.,* 2015b). The detection of clearly secondary, apparently isolated inclusion assemblages within detrital chromite suggests caution should be applied when using this as a line of evidence for the presence of primary inclusions, and instead points to the presence of sub-micron or annealed fractures within grains, or fracturing below the 2D surface shown by electron imaging (*e.g.,* Cavosie *et al.,* 2018).

Our data therefore indicate that inclusion assemblages formed from interaction of detrital chromite and metamorphic fluids within the metasedimentary host. Pitted and porous domains, which are analogous to spongy textures described elsewhere (Gervilla *et al.,* 2012; Colás *et al.,* 2014) and host the same secondary mineral assemblages, were also likely formed by this process. Coarser, euhedral inclusions may reflect direct dissolution of primary inclusion phases, akin to aforementioned replacement of primary inclusion assemblages within detrital zircon (Rasmussen *et al.,* 2011). It is more problematic to prescribe an origin to inclusions of Fe-sulphide and rutile. Sulphide and chromite are commonly co-liquidus phases under iron-sulphide saturated magmatic conditions; however, secondary pyrite is often observed within Jack Hills metasedimentary rocks (*e.g.,* Cavosie *et al.,* 2004; Supplementary Material) and iron-sulphides (typically ≤40 μm pyrite, pyrrhotite, intergrowths of pyrite and pyrrhotite, and rarer

pentlandite) are ubiquitous within isolated quartzite cobbles (Dare *et al.,* 2016). Pyrrhotite, pyrite and rare chalcopyrite inclusions within Jack Hills chromites appear to be closely linked to pitted domains (Fig. 5c); we therefore propose a secondary origin for Fe-sulphide inclusions within chromite.

Inclusions of rutile may be anhedral, globular or preserved as laths aligned to chromite crystallographic axes and are particularly abundant within pitted and porous domains. Observed alignment of alteration phases within chromite (Figs. 4e & 5a) is noted elsewhere, including in chlorite (Fleet *et al.,* 1993; Gervilla *et al.,* 2012) and phlogopite (Rollinson *et al.,* 2002). Whether rutile was precipitated from metamorphic fluids, or was exsolved from chromite, perhaps via changes in the oxidisation state of grains (*e.g.,* Cameron *et al.,* 1979), is unclear. High-Ti domains associated with cracks within zircon (Harrison & Schmitt, 2007; Hofmann *et al.,* 2009), and the secondary growth of rutile within metasedimentary matrix (Harrison *et al.,* 2007) attests to Ti mobility within Jack Hills metasedimentary rocks. While we consider a secondary origin of rutile most likely, we note direct exsolution from chromite that previously had higher TiO_2 contents cannot be discounted.

Chromite mineral chemistry

Signatures of metamorphism

Jack Hills detrital chromites typically yield high ZnO and MnO coupled with low Mg# (typically ≤30; Fig. 6). Chromites with such distinctive chemical compositions are uncommon (*e.g.,* Wylie *et al.,* 1987; Santti *et al.,* 2010; Fanlo *et al.,* 2015) and largely attributed to secondary processes (*e.g.,* Barnes, 2000). A number of studies have investigated the effects of secondary modification of chromite major, minor and trace elements (*e.g.,* Barnes, 2000; González-Jiménez *et al.,* 2009; Mukherjee *et al.,* 2010; 2015; Gervilla *et al.,* 2012; Colás *et al.,* 2014). Hypotheses as to the various processes that modify chromite include: elemental mobility

via interaction with aqueous fluids during the breakdown of surrounding Mg-Fe silicates via serpentinisation (Burkhard, 1993; Marques *et al.,* 2007; Hodel *et al.,* 2017) and/or metamorphism (Barnes, 2000; González-Jiménez *et al.,* 2009; Gervilla *et al.,* 2012; Colás *et al.,* 2014; Fanlo *et al.,* 2015; Ahmed & Surour, 2016), Cu-Zn-Ni-(Co) sulphide mineralisation of the host rock (Wylie, 1987; Marques *et al.,* 2007; Fanlo *et al.,* 2015), and magmatic sulphide mineralisation (Groves *et al.,* 1977). The effects of these processes on chromite chemistry are dependent on the temperature and longevity of alteration, the nature and fO_2 of the aqueous medium, the composition of the host rock and subsequent chromite/silicate ratio, and the fluid/rock ratio during modification (Colás *et al.,* 2014; Ahmed & Surour, 2016). The most commonly observed divalent cation mobility during thermal events is a decrease in Mg#, as Fe^{2+} diffusively enters the chromite lattice at the expense of Mg^{2+} (Barnes, 2000; Colás *et al.,* 2014). ZnO, MnO and to a lesser extent CoO, also diffuse into the chromite lattice in exchange for MgO, NiO and often TiO_2 (Barnes, 2000; Colás *et al.,* 2014).

Within Jack Hills detrital chromites, coupled growth in ZnO content with increasingly homogenised and lowered Mg# likely signifies greater exchange with the modifying medium (Fig. 6a). This may indicate variable modification within their protolith; however, analogous signatures of alteration have been previously reported by Challis et al. (1995), where detrital chromites within fuchsitic sedimentary rocks yielded elevated ZnO (up to 13.7 wt.%) and MnO (up to 3.5 wt.%), coupled with low Mg#. Critically, the detrital grains described by Challis et al. (1995) possessed a well constrained provenance, demonstrating the observed signatures could only have formed during post-depositional metamorphism.

We propose that the dominant signatures of secondary modification within Jack Hills detrital chromites occurred from exchange of grains with metamorphic fluids and/or assemblages during metamorphism of their metasedimentary hosts. Firstly, as established above, interaction of chromite with metamorphic fluids is shown by replacement of inclusion

assemblages (Fig. 5) and the development of pitted and porous domains. Secondly, large differences in chromite chemistry between samples does not relate to the physical characteristics of grains, such as shape or grain size (Supplementary Figs.), but are a function of sampling site and therefore sedimentary horizon. Homogeneity of Mg# (*e.g.,* 16WA7 & 16WA9; Fig. 6) requires modification under the same physiochemical conditions, including temperature, fO_2 and Mg# of modifying medium, despite the probable variation in sedimentary transport characteristics. Observed Mg# uniformity is therefore difficult to reconcile with metamorphic modification with an ultramafic or mafic protolith.

Finally, and most significantly, chromites yield substantial inter-sample chemical variability despite the proximity (often <5 m) of sampling locations (Fig. 2), with the meter-scale variability of ZnO and Mg# of detrital chromites reconciled by changes in grain size and modal proportions of chromite within the host metasedimentary rocks (14WA1-4; Supplementary Material). Chromites are the sole ZnO bearing phase, but are present at low modal proportions of <1 %. As such, minor changes in the modal proportion and grain size of detrital chromites can account for large variations of wt.% ZnO within detrital chromites during interaction and equilibration with secondary fluids. However, 01JH36 detrital chromites, sampled from a heavy mineral layer within which chromites represent a significant component, yield elevated ZnO (2.02 to 4.74 wt.%) within 01JH36 detrital chromites. Simple changes in the modal proportion of chromite therefore cannot account for the ZnO content of grains within this sample. Instead, 01JH36 chromite mineral chemistry may be reconciled by metamorphic equilibration of ZnO at length scales greater than heavy mineral bands (≥ mm-scale) and, given the distance of this sample from the W-74 site (Fig. 2), variable physiochemical compositions of metamorphic fluids across the Jack Hills. Thus, variability in modification signatures may also reflect changing parameters of metamorphic fluids, as also suggested by the often poor correlation between Mg# and MnO with the modal proportion of detrital chromite.

610

611 *Oxygen isotope compositions*

612 *In-situ* modification of chromites is also suggested by oxygen isotope compositions. The
613 variation of δ18O with grain size in chromites from samples 01JH36 and 01JH42 (Fig. 10a-b)
614 indicates they experienced partial exchange of oxygen isotopes with the metasedimentary host
615 rocks. If exchange was by diffusion inwards from the grain boundary, then greater modification
616 of smaller grains is expected given their greater surface area to volume ratio. The lower $\delta^{18}O$
617 values of the smallest chromite grains from 01JH36 and 01JH42 may therefore approach
618 equilibration with host quartz during metamorphism or retrogression. In contrast, chromite
619 grains in sample 01JH54 show no grain size dependence on $\delta^{18}O$ (Fig. 10c). Given the
620 conspicuously lower chromite $\delta^{18}O$ values recorded in 01JH35 and 01JH36, we tentatively
621 interpret chromite $\delta^{18}O$ values in sample 01JH54 as pre-depositonal. Low $\delta^{18}O$ (≤2.5-3.0 ‰)
622 are reported within chromitite from ophiolites and layered intrusions due to exchange with late-
623 stage magmatic and sub-solidus fluids (Lowry *et al.,* 2003; Schannor *et al.,* 2018).

624 The oxygen isotope ratios for smallest chromite size fractions in samples 01JH36 and
625 01JH42 were compared with previously published $\delta^{18}O$ values for quartz in the same samples
626 (Supplementary Table 2; Cavosie *et al.,* 2005). Cavosie *et al.* (2005) found that values of
627 $\delta^{18}O(Qz)$ are homogeneous at hand sample scale in these rocks, indicating metamorphic
628 equilibration of quartz in pebbles and matrix. If attainment of oxygen isotope equilibrium
629 between quartz and chromite is assumed, the $\Delta^{18}O$ value ($\Delta^{18}O_{Quartz\text{-}Chromite} = \delta^{18}O_Q - \delta^{18}O_C$) for
630 samples 01JH36 ($\Delta^{18}O_{Q\text{-}C}$ = 12.02 ‰) and 01JH42 ($\Delta^{18}O_{Q\text{-}C}$ = 12.70 ‰), can be applied to
631 calculate the temperature at which the observed fractionations were established (Zheng *et al.,*
632 1991). Calculated temperatures are 412 °C and 390 °C for samples 01JH36 and 01JH42,
633 respectively. Sample 01JH54 yields a distinctly smaller fractionation ($\Delta^{18}O_{Q\text{-}C}$ = 9.11 ‰) that
634 would correspond to a temperature of 530 °C if it represented metamorphic equilibration.

635 However, as discussed above, the analysis of different sized grains suggests that chromite grains
636 in this sample preserve pre-depositonal $\delta^{18}O$ from and may not be appropriate for metamorphic
637 thermometry. While it cannot be demonstrated that oxygen isotope equilibrium was established
638 between quartz and chromite based on $\delta^{18}O$ analysis of 2 mg aliquots in the other two samples,
639 we note that the derived temperatures based on measured fractionations are consistent with
640 greenschist facies metamorphic conditions previously documented within the Jack Hills
641 (Cavosie *et al.,* 2004; Spaggiari *et al.*, 2007b).

642 Quartz in the metasedimentary rocks analysed has been shown to have recrystallized
643 during metamorphism, and yields homogeneous $\delta^{18}O$ values at >cm scales (Cavosie *et al.,*
644 2005). In contrast, detrital chromites in the same samples preserve detrital morphologies, likely
645 preserve gradients in $\delta^{18}O$ at sub-mm scale (Fig. 10), and are not equilibrated in $\delta^{18}O$. We
646 therefore use the $\delta^{18}O$ values determined for quartz (Cavosie *et al.,* 2005) and temperatures
647 determined from oxygen isotope thermometry to estimate the $\delta^{18}O$ value of fluids present
648 during metamorphism (Supplementary Table 3). Calculated water $\delta^{18}O$ values using quartz-
649 water fractionation factors of Sharp *et al.* (2016) and the published quartz $\delta^{18}O$ values yields
650 water $\delta^{18}O$ values of 8.58 ‰ (at 412 °C) for samples 01JH42 and 8.16 ‰ (at 390 °C) for sample
651 01JH36; a value of water $\delta^{18}O$ of 8.50 ‰ (at 530 °C) for sample 01JH54 is comparable to the
652 other two samples, but may be fortuitous given the lack of evidence for equilibration in sample
653 01JH54 (Fig. 10). Regardless, the range of all calculated water $\delta^{18}O$ values, from 8.2-8.6 ‰,
654 are typical for magmatic or metamorphic fluids (Sheppard, 1986).

655

656 *Trivalent cations: retained primary signatures?*

657 While divalent cations exchange more readily during metamorphism, trivalent cations appear
658 largely immobile during low temperature modification (*e.g.,* Barnes, 2000). Chromite
659 interacting with acidic fluids during sea-floor hydrothermal metasomatism may rarely induce

660 trivalent cation exchange (Wylie *et al.,* 1987; Marques *et al.,* 2007; Hodel *et al.,* 2017); more
661 generally, however, nascent trivalent mobility occurs at greenschist facies metamorphism
662 (Kimball *et al.,* 1990; González-Jiménez *et al.,* 2009) and becomes increasingly pervasive at
663 and above amphibolite facies (Barnes, 2000; González-Jiménez *et al.,* 2009; Colás *et al.,* 2014).
664 Under oxidising conditions, trivalent cation exchange most commonly facilitates the transition
665 of chromite to ferritchromit [$Fe^{2+}(Fe^{3+},Cr)_2O_4$], where Al_2O_3 is lost to Fe_2O_3 either diffusively
666 (Wylie *et al.,* 1987; Gervilla *et al.,* 2012; Colás *et al.,* 2014) or via reaction with magnetite rims
667 (Evans & Frost, 1975; Barnes, 2000). Extensive formation of ferritchromit and Cr-magnetite,
668 and thus modification of chromite core compositions, appears to be largely restricted to
669 amphibolite facies metamorphism and above (Barnes, 2000).

670 Regardless of the degree of secondary modification of divalent cations, Jack Hills
671 detrital chromites possess a broad but consistent range in Cr# across all metasedimentary
672 sample locations (Fig. 7). The range of Cr# may be explained by either the absence of
673 significant trivalent mobility, or the equilibration of chromite during secondary modification
674 with a Cr-Al bearing equilibrant (*e.g.,* fuchsite or metamorphic fluid). If secondary exchange
675 was significant for trivalent cations, the latter scenario should manifest as homogenisation to
676 lower or higher Cr# in increasingly Zn-rich samples. This is not observed. Additionally,
677 zonation profiles of variable Mg# but homogeneous Cr# within low ZnO chromites (Fig. 8a)
678 would require more exchange, and thus faster diffusion, of trivalent than divalent cations. Such
679 an order of relative diffusivities is in strong contrast to previous literature (*e.g.,* Barnes, 2000),
680 and considered extremely unlikely.

681 Unmodified Cr# within chromites is at apparent odds with the presence of surrounding
682 fuchsite, whose elevated Cr content is almost certainly derived from detrital chromites. Fuchsite
683 yields Cr_2O_3 concentrations of ~2-3 wt.% (Cr# <5; Supplementary Table 4), that decrease with
684 increasing distance from detrital chromite grains (e.g., Rasmussen *et al.,* 2011). Such low

concentrations within fuchsite require only minor mobilisation of Cr from chromite, and suggest that the Cr required was scavenged from more heavily altered areas of chromite during metamorphic precipitation of fuchsite, or from dissolution of strongly modified grains in acidic fluids. This is supported by lobate boundaries of detrital chromites with surrounding fuchsite (Fig. 9a-b). Selection of grains with well-defined shapes has likely filtered our dataset for such heavily modified compositions; the process of fuchsite formation causes ragged grain boundaries and extensive fracturing of chromites, which significantly modifies grain morphology (Fig. 3).

Localised zones of Cr-Al mobility may, however, shown by high Cr# domains (Fig. 9), with their generation reconciled via preferential loss of Al during localised exchange between chromite and fuchsite and/or the metamorphic fluid that precipitated fuchsite. High Cr#, low Fe^{3+}# and inclusion free zones of alteration have previously been documented by Arai *et al.* (2006), who suggested such domains represent the loss of Al^{3+} without concurrent addition of Fe^{3+}. Alternatively, high Cr# domains may reflect compositions transitional to ferritchromit or fluid-mediated recrystallisation, although further microstructural analysis would be required to show this. The distinct boundary between the bulk chromite and high Cr# domains (Fig. 9) was suggested by Arai *et al.* (2006) to represent a spinel miscibility gap at high-Cr, Low-Fe^{3+} conditions. Importantly, the sharp gradients indicate negligible diffusion between high Cr# domains and bulk chromites. Therefore, while high Cr# domains clearly represent areas of elevated alteration during metamorphism of host metasedimentary rocks, the retention of sharp boundaries implies an absence of trivalent cation mobility within bulk chromites.

High Cr# domains yield strong compositional similarities to high Cr# chromite, which creates increased uncertainty as to the primary origin of high Cr# grains. However, inter-grain variability in Mg# is still apparent within 14WA2, and the zonation profile of high Cr# 14WA2-PB-12 (Cr# ~75) shows Mg# variability (Supplementary Material Fig. XX); if elevated Cr#

were a product of enhanced trivalent mobility, Mg# heterogeneity should not be observed. This, coupled with the sharp boundaries of high Cr# domains, provides strong evidence that chromite with consistently high and homogeneous in Cr# are pre-depositional in origin.

Timing and cause of chromite modification

It is apparent from the mineral chemistry and inclusion assemblages of Jack Hills detrital chromites that grains were modified within host metasedimentary rocks. However, the timing and magnitude of metamorphic events within the Jack Hills are poorly understood (*e.g.,* Kemp *et al.,* 2018). Previous work has attested to three thermal or fluid flow events within Jack Hills metasedimentary rocks at ca. 2650 Ma, ~1850-1800 Ma and 800 Ma (Spaggiari, 2007a; Rasmussen *et al.,* 2010; 2011; Kemp *et al.,* 2018). Below, we deliberate the timing and magnitude of metamorphic events experienced by Jack Hills detrital chromites.

Dominant metamorphic signatures; a ~2650 Ma event

Metamorphism at ~2650 Ma has been proposed to represent peak metamorphic conditions at the W-74 site (EARLIER PAPER; Rasmussen et al., 2010; 2011). While inclusion assemblages within Jack Hills chromites have not been dated, and so cannot be definitively linked to this event, previous investigation of secondary monazite and xenotime within detrital zircons from the W-74 site observed a large population of this age (Rasmussen *et al.,* 2011). Monazite-xenotime Gd exchange and Ti-in-quartz thermometry indicates metamorphic temperatures of <487 °C at this time, typical of upper greenschist facies metamorphism (Rasmussen *et al.,* 2011). Importantly, temperatures calculated for oxygen isotope equilibrium between chromite and quartz fall within the temperatures anticipated for greenschist facies metamorphism, and also argue for exchange at this time. Given that the ~2650 Ma event represents the highest grade of metamorphism experienced by metasedimentary rocks local to the W-74 site, this event

likely imposed the observed chromite mineral chemistry. The chemical compositions of Jack Hills chromites can therefore be explained by partial to complete exchange with Fe-, Zn- and Mn-bearing metamorphic fluids and mineral assemblages during upper greenschist to lower amphibolite facies metamorphism at ca. 2650 Ma. Metamorphic fluids were likely acidic to facilitate the mobility of Ti^{4+} (*e.g.,* van Baalen, 1993), and enable localised dissolution of chromite to form fuchsite.

This event also coincides with amphibolite to granulite metamorphism throughout the Narryer Terrane, including gneisses adjacent to the belt, and ubiquitous granitic emplacement within the entire Yilgarn Craton (Kemp *et al.,* 2018). This includes the ca. 2650 Ma monzogranite ('The Blob granite'; Pidgeon & Wilde, 1998), which intrudes the Jack Hills belt to the SW of Eranondoo Hill (Fig. 2). Speculatively, this intrusion, or other granitic intrusions adjacent to the Jack Hills belt, may have supplied heat and a metasomatic component (particularly volatile Zn) to metamorphic fluids; similarly modified detrital chromites reported by Challis *et al.* (1995) were postulated to have gained their chemical compositions by interaction with fluids derived from local granitic plutons. An alternative and more local source of ZnO within Jack Hills metasedimentary rocks may come from dissolution of sphalerite (ZnS), which may be a potential detrital phase given the abundance of Fe-sulphides within quartzite cobbles.

Studies have shown that metasedimentary rocks with Proterozoic depositional ages are complexly intercalated with, and at the same apparent metamorphic grade, as metasedimentary associations with inferred Archean depositional ages (Cavosie *et al.,* 2004; Dunn *et al,* 2005; Grange *et al.,* 2010; Wang & Wilde, 2018). This, coupled with ~1850-1800 Ma and ~800 Ma ages within the Jack Hills (Spaggiari et al., 2007b; Rasmussen et al., 2010; 2011), indicates Proterozoic overprinting at a lower metamorphic grade than peak metamorphic conditions.

Subtle zonation trends within some chromites, namely increased Mg# within 14WA4 (Fig. 8b), may be reconciled by minor elemental mobility (Mg, Fe, Zn) within the Proterozoic.

Pre-depositional modification?

Given the susceptibility of chromite to sub-solidus exchange, signatures of modification prior to deposition must also be considered. Divalent cations have undergone significant exchange within host metasedimentary rocks; it is unclear if preservation of high Mg# within the cores of some low ZnO grains (e.g., 14WA2-PB-46; Fig. 6b) represent pre-depositional Mg#, or have still undergone partial exchange. However, pre-depositional metamorphism of accessory chromites (e.g., within their protolith), should result in trivalent cation mobility namely the development of ferritchromit rims (Barnes, 2000; Colás *et al.,* 2014). While the generation of ferritchromit is limited within chromitites, where the higher modal abundance of chromite in chromitite has been shown to inhibit significant metamorphic exchange and thus the generation of ferritchromit (*e.g.,* Mukherjee *et al.,* 2010), chromitite typically represent relatively minor components of igneous bodies (Barnes & Roeder, 2001). Given the presence of EO, which have undergone little abrasion and rounding during sedimentary reworking, ferritchromit or magnetite rims should be clearly visible if present prior to deposition. No ferritchromit has been observed within this study, providing evidence chromites have not undergone resolvable trivalent mobility prior to erosion from their protoliths. While we cannot definitively exclude trivalent cation mobility prior to deposition, we suggest that Cr# of Jack Hills detrital chromites represent the most robust chemical signature for investigation of provenance.

Provenance

While detrital chromites exhibit protracted metamorphic histories, some chemical signatures place constraints on the magmatic protolith. Consistent variability of Cr# regardless

784 of shape may indicate a common mafic or ultramafic protolith. While we base this
785 interpretations on least altered chromites within samples 14WA2 and 01JH54, the consistent
786 range of chromite Cr# from all 14WA, 16WA and 01JH metasedimentary rocks analysed
787 potentially suggests that a single, large-scale magmatic source potentially dominated the mafic
788 and ultramafic crust within the catchment of the Jack Hills sedimentary rocks. Unfortunately,
789 important chemical tools for understanding the petrogenesis of chromite and consequently their
790 protolith, namely Mg# and TiO_2, are not appropriate to apply to Jack Hills detrital chromites
791 due to modification within host metasedimentary rocks. Therefore, commonly used plots for
792 chromite provenance, such as TiO_2 vs Cr_2O_3 or Al_2O_3 (Kamenetsky *et al.,* 2001), are unlikely
793 to be reliable. We propose trivalent cation mobility was limited within Jack Hills detrital
794 chromites, but cannot fully exclude metamorphic re-equilibration of $Fe^{3+}/\Sigma R^{3+}$ prior to
795 deposition. We therefore suggest careful use of $Fe^{3+}/\Sigma R^{3+}$ may provide better insights into the
796 provenance of Jack Hills chromites; unmistakably non-stoichiometric grains (*i.e.,* $Fe^{3+} = <0$)
797 from 14WA2 are excluded Fig. 13 for clarity. The retention of unmodified Cr# within cores of
798 Jack Hills chromite will therefore yield the most information on provenance of detrital grains,
799 alongside careful and conservative use of $Fe^{3+}/\Sigma R^{3+}$ and, where rutile laths are demonstrably
800 absent, TiO_2 contents.

801 To gain understanding of the petrogenesis of Jack Hills detrital chromites, and
802 potentially of mafic and ultramafic crust within the Narryer Terrane, we use the fields of Barnes
803 & Roeder (2001), a comparative study of over 26,000 spinels from different tectonic settings.
804 We compare these fields to grains from 14WA2 and 01JH54, which, due to low ZnO coupled
805 with partial exchange of Mg#, we interpret to represent the least altered compositions of detrital
806 chromite. We do not include the chemical compositions of chromitites within the fields of Figs.
807 10-13; chromitites compromise a low volumetric component of igneous bodies, particularly
808 layered intrusions, and have been suggested to induce bias within provenance studies (Power

809 *et al.,* 2000; Barnes & Roeder, 2001). While 14WA2 appear conform to a Cr-Al trend (Fig. 11;
810 Irvine, 1967; Barnes & Roeder, 2001), where no enrichment of Fe^{3+} is observed with changing
811 Cr#, this likely reflects non-stoichiometry. The consistently low ferric iron contents of 01JH54
812 chromites are not suggestive of Fe-Ti or Rum trends (Fig. 11), which form via the reaction of
813 plutonic chromites with intercumulus liquid enriched in both Fe^{3+} and Ti.

814 As expected, in Cr# vs. Fe^{2+}# (inverse Mg#) compositional space, Jack Hills detrital
815 chromites fall within the 90th percentile of spinel within high grade metamorphic rocks (Fig.
816 12a). The decrease of Mg# within Jack Hills detrital chromites due to metamorphic exchange
817 results in comparable Mg# to chromites modified within mafic-ultramafic protoliths; this
818 process is also shown in Fig. 12d, where an increase in metamorphic grade from greenschist to
819 amphibolite facies results in significantly lowered and homogenised Mg# within komatiitic
820 chromites. While superficially Jack Hills detrital chromites yield a similar Cr# variability to
821 those modified by metamorphism, the range in Cr# shown within the metamorphic field (Fig.
822 12a) represents compositions transitional from magmatic Cr# to ferritchromit and magnetite.
823 As such alteration phases are absent within Jack Hills chromites, and zonation profiles show
824 limited Cr# variability, this process cannot explain the fit of grains to the metamorphic field of
825 Barnes & Roeder (2001). A different provenance is therefore required for the observed Cr#.

826 The variable and moderate to high Cr# of Jack Hills detrital chromites (typically 55-70)
827 are comparable to ophiolitic chromites (Fig. 12b), continental layered intrusions (Fig. 12c), and
828 intra-plate settings such as ocean island tholeiites and oceanic plateaus (Dick & Bullen, 1984;
829 Barnes & Roeder, 2001; Arai *et al.,* 2011). Critically, the Cr# of Jack Hills chromites indicate
830 the majority of detrital grains cannot be derived from komatiites (Fig. 12d). As a product of
831 high temperature and high degree mantle melts, komatiites have high Cr/Al ratios and therefore
832 yield chromite with high Cr# (typically >70; Barnes & Roeder, 2001) that yield tightly clustered
833 compositions due to the inhibition of magmatic fractionation or subsolidus equilibration. In

834 comparison to both Al-undepleted komatiites (AUDK; Fig. 12d) and Al-depleted komatiites
835 (ADK), Jack Hills detrital chromites yield more variable and moderate Cr# (typically 55-70).
836 ADK are not shown in Fig. 12 as they yield chromite with too high Cr# (>85) to represent a
837 source of Jack Hills detrital chromite. Some portions of komatiitic lavas, such as olivine-rich
838 dunitic channels and sheets, have been shown to yield chromite with lower Cr# (60-70) than
839 bulk ADK and AUDK (Barnes, 1998; Barnes & Roeder, 2001). However, chromite is not
840 abundant in these reduced cumulates, and would be unlikely to dominate the detrital record
841 over their bulk komatiitic counterparts.

842 We suggest that, on the basis of Cr#, the most likely provenance of Jack Hills detrital
843 chromites is a layered intrusion. Notably, though chromitite fields are not included in Fig. 12
844 and Fig. 13, Jack Hills detrital chromites yield comparable Cr# to Stillwater 'G' and Bushveld
845 chromitites (*e.g.,* Campbell & Murck, 1993; Langa et al., 2020 and references therein). While
846 variable chromite morphologies may reflect different transport mechanisms, an absence of
847 chemical variation with rounding shape of grains may be further qualitative evidence of a
848 potential layered intrusion source; layered intrusions may yield consistent lithologies and
849 mineral chemistry laterally for many kilometres. In the absence of definitive Fe_2O_3 or TiO_2
850 concentrations, tectonic settings with comparable Cr#, including podiform and other mantle
851 derived Cr-spinel, cannot be excluded (as shown by ophiolites; Fig. 13a). Thus, while we
852 consider a layered intrusive source the most likely source of Jack Hills detrital chromites,
853 further investigation of additional chemical signatures may provide evidence for or against this
854 interpretation.

855 However, chromite from early Archean anorthositic layered intrusions yield marked
856 physiochemical differences to those from stratiform complexes, which dominate the layered
857 intrusion fields of Fig. 12 and Fig. 13. Archean anorthositic layered intrusions typically form
858 sill-like bodies that are significantly less volumetric than Proterozoic massif-type anorthositic

intrusions, and are thought to represent sub-volcanic intrusions coeval to overlying greenstone belts (*e.g.,* Ashwal & Bybee, 2017). Archean sill-like anorthositic intrusions yield spinel that are typically Fe rich, with populations of high Cr# (>70) or low Cr# (<50) (Rollinson *et al.,* 2002; 2010; Mondal *et al.,* 2006; Dharma Rao *et al.,* 2013; Mukherjee *et al.,* 2015; Rowe & Kemp, 2020), thought to reflect derivation from parental melts of komatiitic, boninitic or hydrous basaltic compositions (Ashwal & Bybee, 2017). Thus, typical mineral chemistry of anorthositic layered intrusive chromites are not comparable to Jack Hills chromites. While chromites extending to Cr# comparable to Jack Hills detrital chromites are documented (*e.g.,* Mukherjee *et al.,* 2010), they typically represent a minor component of bulk chromite compositions. As with chromites from komatiitic dunitic channels, such chromites are unlikely to dominate detrital records over higher Cr# counterparts.

While Jack Hills detrital chromites do not yield Cr# equivalent to Cr-spinel from sill-like Archean anorthositic layered intrusions, chromite from late Archean layered intrusions with comparable chemical compositions are known (*e.g.,* Rollinson *et al.,* 2010; Berger *et al.,* 2013; Szilas *et al.,* 2017). The development of massif-type anorthositic intrusions at the beginning of the Proterozoic are thought to coincide with the emergence of increasingly thickened and strengthened lithosphere, a consequence of secular cooling and potentially shifting geodynamic regimes (Ashwal & Bybee, 2017). This therefore does not exclude the presence of more massif-type layered intrusions during the early Archean; the preservation potential of larger, and thus higher density, stratiform intrusions would be significantly lower in the presence of hotter Archean mantle.

Potential sources within the Narryer Terrane

As the mineral chemistry of Jack Hills detrital chromites allude to a layered intrusion origin, and unpublished Re-Os isotopic data yield model ages that are at least Palaeoarchean in age

884 (Valley *et al.,* 2005), the sole described layered intrusion within the Narryer Terrane, the 3730
885 Ma Manfred Complex (Kinny *et al.,* 1988; Fletcher *et al.,* 1988; Myers, 1988b; Rowe & Kemp,
886 2020), can be considered as a potential source. Spinel within the Manfred Complex is
887 dominantly spinel *sensu stricto* or picotite, and occurs closely associated with magmatic olivine
888 (Rowe & Kemp, 2020) or exsolved from cumulus orthopyroxene or clinopyroxene. Chromite
889 is completely absent in the Manfred Complex harzburgites and websterites studied by Rowe &
890 Kemp (2020); however, metaperidotites within the Manfred Complex contain chromite
891 (Fletcher *et al.,* 1988; Myers, 1988b; Kemp *et al.,* 2018). Here, we compare the least altered
892 14WA2 and 01JH54 detrital grains with chromites from Manfred Complex sample 13TKN22
893 (Supplementary Material), a pyroxene-phyric peridotite metamorphically modified to
894 hornblende and altered to serpentine.
895 13TKN22 chromites (n=13 analyses) occur as disseminated crystals with variably
896 formed magnetite rims (Fig. 14a-b), and yield consistent Cr# of 76-80 (Table 2), coupled with
897 low Mg# of <20, likely reflecting metamorphism of the host metaperidotite. 13TKN22
898 chromites yield limited ZnO (~0.6 wt.%) and heterogeneous MnO (0.4-1.4 wt.%). NiO is
899 present at magmatic concentrations of >0.1 wt.%, but this may reflect the high magnetite
900 component of 13TKN22 chromites (Barnes, 1998). While divalent cation mineral chemistry
901 suggests metamorphic alteration of 13TKN22 chromites, the sharpness of the boundary
902 between chromite cores and magnetite rims (Fig. 14a-b) and the tightly clustered compositions
903 of cores (Fig. 14d-e) indicate restricted trivalent mobility (*e.g.,* Barnes, 2000). While the highest
904 Cr# Jack Hills detrital grains overlap with the Cr# of 13TKN22 chromites (Fig. 14), detrital
905 chromites possess significantly lower ferric iron contents and TiO_2, though given the
906 uncertainties introduced by Ti mobility within host metasedimentary rocks comparisons should
907 be taken tentatively. 13TKN22 chromites therefore cannot account for the bulk population of
908 Jack Hills chromite detrital grains, which possess lower Cr#, and these lithologies did not

represent the dominant component of mafic to ultramafic crust within the erosional catchment of Jack Hills metasedimentary rocks.

While mafic and ultramafic crust within the Narryer Terrane tends to be collectively grouped as the Manfred Complex, more recent geochronological investigations have shown many of these lithologies actually have Paleoarchean igneous crystallisation ages (Kemp *et al.,* 2018). Continued investigation of these units may reveal further insights into the provenance of Jack Hills detrital chromites. Mafic and ultramafic rocks that occur within the Jack Hills belt may also represent the source for Jack Hills detrital chromites, particularly given the proximal source suggested for EO. Jack Hills mafic and ultramafic rocks are heavily sheared and extensively recrystallised (Spaggiari, 2007a), however analysis of one sample (16WA13; Supplementary Material) found relict chromite cores within texturally distinct chromite stringers. Whether this texture is igneous or deformational in origin is unclear, but the development of thick and indistinct magnetite and ferritchromit rims (Fig. 14c-d) yields evidence for at least amphibolite facies metamorphism (*e.g.,* Barnes, 2000), likely representing amphibolites facies metamorphism of the Jack Hills belt prior to deposition of Unit 3 and 4 metasedimentary rocks (Spaggiari *et al.,* 2007a/b). While 16WA13 relict cores possess comparable Cr# to some Jack Hills detrital grains, gradational and lobate boundaries between relict cores and ferritchromit-magnetite rims, and their compositional trend towards magnetite (Fig. 14) are evidence for mobility of trivalent cations. This indicates that the Cr# of 16WA13 chromite cores represent maximum values, and that comparisons should be taken cautiously. However, further analyses of Jack Hills mafic and ultramafic rocks, particularly those preserved within lower strain areas, may prove more fruitful.

CONCLUSIONS

933 We have conducted a detailed textural and chemical investigation of detrital chromite from the
934 Jack Hills, Western Australia, in a bid to expand beyond the intensively studied zircon record
935 and provide additional perspectives on sources of sedimentary detritus (Fig. 15). Detrital
936 chromites have undergone modification during metamorphism of host metasedimentary rocks,
937 with significant mobility of divalent cations. This is shown by increasingly homogenised and
938 lowered Mg#, elevated ZnO and MnO, and partial to complete exchange of oxygen isotopes.
939 Interaction with metamorphic fluids also resulted in the generation of pitted domains and
940 replacement of primary mineral assemblages with metamorphic phases present in the matrix of
941 host metasedimentary rocks, dominantly quartz and fuchsite. We propose metamorphic
942 modification coincided with peak upper greenschist to lower amphibolite facies metamorphism
943 of Jack Hills metasedimentary rocks at ~2650 Ma.

944 Despite the development of fuchsite and high Cr# domains, Jack Hills chromites yield
945 a consistent range in Cr# across all samples and have limited intra-grain variability, indicating
946 the Cr# of chromites cores are robust. An absence of ferritchromit rims on euhedral grains
947 further argues against significant trivalent mobility prior to deposition. Critically, the moderate
948 and variable Cr# of most detrital chromites suggest that komatiites or associated intrusives were
949 not a significant component of mafic-ultramafic crust within the erosional catchment of Jack
950 Hills metasedimentary rocks. We propose a layered intrusive origin for Jack Hills detrital
951 chromites, though note that in the absence of further constraints from ferric iron and TiO_2
952 contents other sources cannot be excluded. It is currently unclear whether detrital chromites
953 represent the remnants of a hitherto unknown intrusion, or were sourced from the 3730 Ma
954 Manfred Complex or from ultramafic horizons within the Jack Hills belt. The lack of significant
955 komatiite contribution may have geodynamic implications for eruption efficiencies within the
956 catchment of Jack Hills sediments (*e.g.,* heat-pipe vs. 'plutonic squishy lid'; Moore & Webb,

957 2013; Rozel *et al.,* 2017), and more broadly, the tectonic distribution of mafic and ultramafic
958 crust within the Archean.

959 While this study focused on Jack Hills detrital chromites, we have demonstrated that
960 with a careful and detailed approach, characteristics of the igneous precursors of detrital
961 chromites may be determined. However, we show that identification of key physiochemical
962 signatures of chromite modification are critical to assess the veracity of interpretations derived
963 from detrital chromites preserved within Archean metasedimentary rocks. Future studies of
964 Archean detrital chromites should ideally be restricted to mature metasedimentary units that
965 have undergone at most lower amphibolite facies metamorphism to minimise trivalent cation
966 mobility. Where alteration of key physiochemical signatures can be shown to be absent, Cr#,
967 Fe_2O_3 and TiO_2 contents may be used to provide significant insights into the provenance of
968 mafic or ultramafic protoliths. Fuchsitic metasedimentary rocks are commonly reported within
969 Archean terranes (*e.g.,* Randive *et al.,* 2015), indicating that the eroded remnants of mafic and
970 ultramafic crust are abundant. Detrital chromites within fuchsitic metasedimentary rocks may
971 therefore represent an innovative tool in understanding the distribution of eroded Archean mafic
972 and ultramafic crust, and yield important insights into geodynamic regimes of the early Earth.

973

974 Funding

975 This work was supported by a Natural Environment Research Council (NERC) GW4+ Doctoral
976 Training Partnership studentship [Grant number S117831-117] and British Geological Survey
977 (BGS) University Funding Initiative (BUFI) sponsorship [Grant number S118481-101] to L.G
978 Staddon. J.W. Valley is funded by the European Research Council [Synergy Grant number
979 856555] and the U.S. National Science Foundation [EAR-1524336].

980

981 Acknowledgements

L.G. Staddon wishes to thank Stuart Kearns and Ben Buse for their assistance with EPMA work, as well as Matthew Rowe and Chris Gray for their help during fieldwork in the Narryer Terrane. Thorough reviews from anonymous reviewers greatly improved this manuscript.

References

Ahmed, A. H. & Surour, A. A. (2016). Fluid-related modifications of Cr-spinel and olivine from ophiolitic peridotites by contact metamorphism of granitic intrusions in the Ablah area, Saudi Arabia. *Journal of Asian Earth Sciences* 122, 58-79.

Amelin, Y., Lee, D. C., Halliday, A. N. & Pidgeon, R. T. (1999). Nature of the Earth's earliest crust from hafnium isotopes in single detrital zircons. *Nature* 399, 252-255.

Arai, S., Okamura, H., Kadoshima, K., Tanaka, C., Suzuki, K. & Ishimaru, S. (2011). Chemical characteristics of chromian spinel in plutonic rocks: Implications for deep magma processes and discrimination of tectonic setting: Chromian spinel in plutonic rocks. *Island Arc* 20, 125–137.

Arai, S., Shimizu, Y., Ismail, S. A. & Ahmed, A. H. (2006). Low-T formation of high-Cr spinel with apparently primary chemical characteristics within podiform chromitite from Rayat, northeastern Iraq. *Mineralogical Magazine* 70, 499–508.

Arndt, N. T., Lesher, C. & Barnes, S. J. (2008). Brief descriptions of six classic komatiite occurrences. *Komatiite*. Cambridge: Cambridge University Press, 16-52.

Ballhaus, C., Berry, R.F., & Green, D.H. (1991). High pressure experimental calibration of the olivine-orthopyroxene-spinel oxygen geobarometer: implications for the oxidation state of the upper mantle. *Contributions to Mineralogy and Petrology* 107, 27-40.

Barkov, A. Y., Nixon, G. T., Levson, V. M., Martin, R. F. & Fleet, M. E. (2013). Chromian spinel from PGE-bearing placer deposits, British Colombia, Canada: Mineralogical associations and provenance. *Canadian Mineralogist* 51, 501-536.

1007 Barnes, S. J. (2000). Chromite in komatiites, II. modification during greenschist to mid-
1008 amphibolite facies metamorphism. *Journal of Petrology* 41, 387-409.
1009 Barnes, S. J. (1998). Chromite in Komatiites, 1. Magmatic Controls on Crystallization and
1010 Composition. *Journal of Petrology* 39, 1689–1720.
1011 Barnes, S. J. & Roeder, P. L. (2001). The range of spinel compositions in terrestrial mafic and
1012 ultramafic rocks. *Journal of Petrology* 42, 2279-2302.
1013 Bell, E. A., Boehnke, P., Harrison, T. M., & Mao, W. L. (2015). Potentially biogenic carbon
1014 preserved in a 4.1 billion-year-old zircon. (2015a). *Proceedings of the National*
1015 *Academy of Sciences of the United States of America* 112 (47), 14518-14521.
1016 Bell, E. A., Boehnke, P., Hopkins-Wielicki, M. D. & Harrison, T. M. (2015b). Distinguishing
1017 primary and secondary inclusion assemblages in Jack Hills zircons. *Lithos* 234, 15-26.
1018 Bell, E. A., Harrison, T. M., Kohl, I. E. & Young, E. D. (2014). Eoarchean crustal evolution of
1019 the Jack Hills zircon source and loss of Hadean crust. *Geochimica et Cosmochimica*
1020 *Acta* 146, 27-42.
1021 Bell, E. A., & Harrison, T. M. (2013). Post-Hadean transitions in Jack Hills zircons: a signal of
1022 the late heavy bombardment? *Earth and Planetary Science Letters* 364, 1-11.
1023 Berger, J., Diot, H., Lo, K., Ohnenstetter, D., Femenias, O., Pivin, M., Demaiffe, D., Bernard,
1024 A. & Charlier, B. (2013). Petrogenesis of Archean PGM-bearing chromitites and
1025 associated ultramafic-mafic-anorthositic rocks from the Guelb el Azib layered complex
1026 (West African craton, Mauritania). *Precambrian Research* 224, 612-628.
1027 Borlina, C. S., Weiss, B. P., Lima, E. A., Tang, F., Taylor, R. J. M., Einslie, J. F., Harrison, R.
1028 J., Fu, R. R., Bell, E. A., Alexander, E. W., Kirkpatrick, H. M., Wielicki, M. M.,
1029 Harrison, T. M., Ramezani, J., & Maloof, A. C. (2020). Reevaluating the evidence for
1030 a Headean-Eoarchean dynamo. *Science Advances* 6 (15), eeav9634. DOI:
1031 10.1126/sciadv.aav9634.

1032 Burkhard, D. J. M. (1993). Accessory chromium spinels: Their coexistence and alteration in
1033 serpentinites. *Geochimica et Cosmochimica Acta* 57, 1297–1306.
1034 Byerly, B. L., Lowe, D. R., Drabon, N., Coble, M. A., Burns, D. H. & Byerly, G. (2018). Hadean
1035 zircon from a 3.3 Ga sandstone, Barberton greenstone belt, South Africa. *Geology* 46,
1036 1-4.
1037 Cameron, E. N. (1979). Titanium-bearing oxide minerals of the critical zone of the eastern
1038 Bushveld Complex. *American Mineralogist* 64, 140-150.
1039 Cameron, E., Valley, J. W., Ortiz-Cordero, D., Kitajima, K., & Cavosie, A. J. (2016). Detrital
1040 Jack Hills zircon-quartz $\delta^{18}O$ analysis tests alteration of zircon and zircon inclusions.
1041 *Goldschmidt Conference 2016,* 349.
1042 Campbell, I. H., & Murck, B. W. (1993). Petrology of the G and H Chromitite Zones in the
1043 Mountain View Area of the Stillwater Complex, Montana. *Journal of Petrology* 34 (2),
1044 291-316.
1045 Cassidy, K. F., Champion, D. C., Krapez, B., Barley, M.E., Brown, S. J. A., Blewett, R. S.,
1046 Groenewald, N. B., & Tyler, I. M. (2006). A Revised Geological Framework for the
1047 Yilgarn Craton. *Geological Survey of Western Australia* (Record 2006/8).
1048 Cavosie, A. J., Valley, J. W., & Wilde, S. A. (2018). The Oldest Terrestrial Mineral Record:
1049 Thirty Years of Research on Hadean Zircon from Jack Hills, Western Australia. In: van
1050 Kranendonk, M. J., Bennett, V. C., and Hoffmann, J. E., (ed.) *Earth's Oldest Rocks*:
1051 Elsevier, 255-273.
1052 Cavosie, A. J., Valley, J. W., & Wilde, S. A. (2005). Magmatic delta O-18 in 4400-3900 Ma
1053 detrital zircons: A record of the alteration and recycling of crust in the Early Archean.
1054 *Earth and Planetary Science Letters* 235, 663-681.

1055 Cavosie, A. J., Wilde, S. A., Liu, D. Y., Weiblen, P. W. & Valley, J. W. (2004). Internal zoning
1056 and U-Th-Pb chemistry of Jack Hills detrital zircons: a mineral record of early Archean
1057 to Mesoproterozoic (4348-1576 Ma) magmatism. *Precambrian Research* 135, 251-279.
1058 Cavosie, A. J., Valley, J. W., Fournelle, J. & Wilde, S. A. (2002). Implications for sources of
1059 Jack Hills metasediments: detrital chromite. *Goldschmidt 2002*, 125.
1060 Challis, A., Grapes, R. & Palmer, K. (1995). Chromian muscovite, uvarovite, and zincian
1061 chromite: Products of regional metasomatism in northwest Nelson, New Zealand.
1062 *Canadian Mineralogist* 33, 1263-1284.
1063 Chaudhuri, T., Wan, Y., Mazumder, R., Ma, M. & Liu, D. (2018). Evidence of Enriched,
1064 Hadean Mantle Reservoir from 4.2-4.0 Ga zircon xenocrysts from Paleoarchean TTGs
1065 of the Singhbhum Craton, Eastern India. *Scientific Reports* 8.
1066 Colás, V., González-Jiménez, J. M., Griffin, W. L., Fanlo, I., Gervilla, F., O'Reilly, S. Y.,
1067 Pearson, N. J., Kerestedjian, T. & Proenza, J. A. (2014). Fingerprints of metamorphism
1068 in chromite: New insights from minor and trace elements. *Chemical Geology* 389, 137-
1069 152.
1070 Compston, W. & Pidgeon, R. T. (1986). Jack Hills, evidence of more very old detrital zircons
1071 in Western Australia. *Nature* 321, 766-769.
1072 Cox, M. A., Cavosie, A. J., Reddy, S. M., Bland, P. A., & Valley, J. W. (2017). The hunt for
1073 shocked zircon in the Jack Hills: 21,000 and counting… *Lunar and Planetary Science*
1074 *2017,* 1402.
1075 Crowley, J. L., Myers, J. S., Sylvester, P. J. & Cox, R. A. (2005). Detrital zircon from the Jack
1076 Hills and Mount Narryer, Western Australia: Evidence for diverse >4.0 Ga source rocks.
1077 *Journal of Geology* 113, 239-263.
1078 Dare, M. S., Tarduno, J. A., Bono, R. K., Cottrell, R. D., Beard, J. S. & Kodama, K. P. (2016).
1079 Detrital magnetite and chromite in Jack Hills quartzite cobbles: Further evidence for the

preservation of primary magnetizations and new insights into sediment provenance. *Earth and Planetary Science Letters* 451, 298-314.

Dharma Rao, C. V., Santosh, M., Sajeev, K., & Windley, B. F. (2013). Chromite–silicate chemistry of the Neoarchean Sittampundi Complex, southern India: Implications for subduction-related arc magmatism. *Precambrian Research* 227, 259-277.

Dhuime, B., Wuestefeld, A. & Hawkesworth, C. J. (2015). Emergence of modern continental crust about 3 billion years ago. *Nature Geoscience* 8, 552-555.

Dick, H. J. B. & Bullen, T. (1984). Chromian spinel as a petrogenetic indicator in abyssal and alpine-type peridotites and spatially associated lavas. *Contributions to Mineralogy and Petrology* 86, 54-76.

Dott, R. H. (2003). The importance of eolian abrasion in supermature quartz sandstones and the paradox of weathering vegetation-free landscapes. *The Journal of Geology* 111 (4), 387-405.

Droop, G. (1987). A general equation for estimating Fe-3+ concentrations in ferromagnesian silicates and oxides from microprobe analyses, using stoichiometric criteria. *Mineralogical Magazine* 51, 431-435.

Dunn, S. J., Nemchin, A. A., Cawood, P. A. & Pidgeon, R. T. (2005). Provenance record of the Jack Hills metasedimentary belt: Source of the Earth's oldest zircons. *Precambrian Research* 138, 235-254.

Fanlo, I., Gervilla, F., Colás, V. & Subias, I. (2015). Zn-, Mn- and Co-rich chromian spinels from the Bou-Azzer mining district (Morocco): Constraints on their relationship with the mineralizing process. *Ore Geology Reviews* 71, 82-98.

Fleet, M. E., Angeli, N. & Pan, Y. M. (1993). Oriented chlorite lamellae in chromite from the Pedra-Branca mafic-ultramafic complex, Ceara, Brazil. *American Mineralogist* 78, 68-74.

1105 Fletcher, I. R., Rosman, K. J. R. & Libby, W. G. (1988). Sm-Nd, Pb-Pb and Rb-Sr
1106 geochronology of the Manfred Complex, Mount Narryer, Western Australia.
1107 *Precambrian Research* 38, 343-354.
1108 Froude, D. O., Ireland, T. R., Kinny, P. D., Williams, I. S., Compston, W., Williams, I. R. &
1109 Myers, J. S. (1983). Ion microprobe identification of 4,100-4,200 Myr-old terrestrial
1110 zircons. *Nature* 304, 616-618.
1111 Gervilla, F., Padrón-Navarta, J. A., Kerestedjian, T., Sergeeva, I., González-Jiménez, J. M. &
1112 Fanlo, I. (2012). Formation of ferrian chromite in podiform chromitites from the
1113 Golyamo Kamenyane serpentinite, Eastern Rhodopes, SE Bulgaria: a two-stage
1114 process. *Contributions to Mineralogy and Petrology* 164, 643-657.
1115 González-Jiménez, J. M., Kerestedjian, T., Proenza, J. A. & Gervilla, F. (2009). Metamorphism
1116 on Chromite Ores from the Dobromirtsi Ultramafic Massif, Rhodope Mountains (SE
1117 Bulgaria). *Geologica Acta* 7, 413-429.
1118 Grange, M. L., Wilde, S. A., Nemchin, A. A., & Pidgeon, R. T. (2010). Proterozoic events
1119 recorded in quartzite cobbles at Jack Hills, Western Australia: New constraints on
1120 sedimentation and source of >4Ga zircons. *Earth and Planetary Science Letters* 292 (1-
1121 2), 158-169.
1122 Groves, D. I., Barrett, F. M., Binns, R. A. & McQueen, K. G. (1977). Spinel phases associated
1123 with metamorphosed volcanic-type iron-nickel sulfide ores from Western Australia.
1124 *Economic Geology* 72, 1224-1244.
1125 Harrison, T. M., Bell, E. A. & Boehnke, P. (2017). Hadean Zircon Petrochronology.
1126 *Petrochronology: Methods and Applications* 83, 329.
1127 Harrison, T. M. & Schmitt, A. K. (2007). High sensitivity mapping of Ti distributions in Hadean
1128 zircons. *Earth and Planetary Science Letters* 261, 9-19.

1129 Harrison, T. M., Schmitt, A. K., McCulloch, M. T. & Lovera, O. M. (2008). Early (≥4.5 Ga)
1130 formation of terrestrial crust: Lu-Hf, $\delta^{18}O$, and Ti thermometry results for Hadean
1131 zircons. *Earth and Planetary Science Letters* 268, 476-486.
1132 Harrison, T. M., Trail, D., Schmitt, A. K. & Watson, E. B. (2007). Rutile ^{207}Pb-^{206}Pb ages in
1133 the Jack Hills quartzite, Western Australia. *Goldschmidt 2007,* A383.
1134 Hodel, F., Macouin, M., Triantafyllou, A., Carlut, J., Berger, J., Rousse, S., Ennih, N. &
1135 Trindade, R. I. F. (2017). Unusual massive magnetite veins and highly altered Cr-spinels
1136 as relics of a Cl-rich acidic hydrothermal event in Neoproterozoic serpentinites (Bou
1137 Azzer ophiolite, Anti-Atlas, Morocco). *Precambrian Research* 300, 151-167.
1138 Hofmann, A. E., Valley, J. W., Watson, E. B., Cavosie, A. J., & Eiler, J. M. (2009). Sub-micron
1139 scale distributions of trace elements in zircon. *Contributions to Mineralogy and*
1140 *Petrology* 158, 317-335.
1141 Hopkins, M., Harrison, T. M. & Manning, C. E. (2008). Low heat flow inferred from >4 Gyr
1142 zircons suggests Hadean plate boundary interactions. *Nature* 456, 493-496.
1143 Hopkins, M. D., Harrison, T. M. & Manning, C. E. (2010). Constraints on Hadean geodynamics
1144 from mineral inclusions in >4 Ga zircons. *Earth and Planetary Science Letters* 298,
1145 367-376.
1146 Hopkins, M., Harrison, T. M. & Manning, C. E. (2012). Metamorphic replacement of mineral
1147 inclusions in detrital zircon from Jack Hills, Australia: Implications for the Hadean
1148 Earth. *Geology* 40, e281.
1149 Iizuka, T., McCulloch, M. T., Komiya, T., Shibuya, T., Ohta, K., Ozawa, H., Sugimura, E. &
1150 Collerson, K. D. (2010). Monazite geochronology and geochemistry of meta-sediments
1151 in the Narryer Gneiss Complex, Western Australia: constraints on the tectonothermal
1152 history and provenance. *Contributions to Mineralogy and Petrology* 160, 803-823.

1153 Iizuka, T., Horie, K., Komiya, T., Maruyama, S., Hirata, T., Hidaka, H. & Windley, B. F.
1154 (2006). 4.2 Ga zircon xenocryst in an Acasta Gneiss from northwestern Canada:
1155 Evidence for early continental crust. *Geology* 34, 245-248.
1156 Irvine, T. N. (1967). Chromian spinel as a petrogenetic indicator part 2: Petrologic application.
1157 *Canadian Journal of Earth Sciences* 4, 71-103.
1158 Irvine, T. N. (1965). Chromian spinel as a petrogenetic indicator part 1: Theory. *Canadian*
1159 *Journal of Earth Sciences* 2, 648-672.
1160 Kamber, B. (2015). The evolving nature of terrestrial crust from the Hadean, through the
1161 Archaean, into the Proterozoic. *Precambrian Research* 258, 48-82.
1162 Kamenetsky, V. S., Crawford, A. J. & Meffre, S. (2001). Factors controlling chemistry of
1163 magmatic spinel: An empirical study of associated olivine, Cr-spinel and melt
1164 inclusions from primitive rocks. *Journal of Petrology* 42, 655-671.
1165 Kamperman, M., Danyushevsky, L. V., Taylor, W. R. & Jablonski, W. (1996). Direct oxygen
1166 measurements of Cr-rich spinel: Implications for spinel stoichiometry. *American*
1167 *Mineralogist* 81, 1186-1194.
1168 Kemp, A. I. S., Wilde, S. A., & Spaggiari, C. (2018). The Narryer Terrane, Yilgarn Craton,
1169 Western Australia: Review and Recent Developments. In: van Kranendonk, M. J.,
1170 Bennett, V. C., and Hoffmann, J. E., (ed.) *Earth's Oldest Rocks*: Elsevier, 401-429.
1171 Kemp, A. I. S. (2018). Early earth geodynamics: cross examining the geological testimony.
1172 *Philosophical Transactions of the Royal Society A* 376.
1173 Kemp, A. I. S., Wilde, S. A., Hawkesworth, C. J., Coath, C. D., Nemchin, A., Pidgeon, R. T.,
1174 Vervoort, J. D. & DuFrane, S. A. (2010). Hadean crustal evolution revisited: New
1175 constraints from Pb-Hf isotope systematics of the Jack Hills zircons. *Earth and*
1176 *Planetary Science Letters* 296, 45-56.

1177 Kimball, K. L. (1990). Effects of hydrothermal alteration on the compositions of chromian
1178 spinels. *Contributions to Mineralogy and Petrology* 105, 337-346.
1179 Kinny, P. D. & Nutman, A. P. (1996). Zirconology of the Meeberrie Gneiss, Yilgarn Craton,
1180 Western Australia: An early Archaean migmatite. *Precambrian Research* 78, 165-178.
1181 Kinny, P. D., Wijbrans, J. R., Froude, D. O., Williams, I. S. & Compston, W. (1990). Age
1182 constraints on the geological evolution of the Narryer Gneiss Complex, Western
1183 Australia. *Australian Journal of Earth Sciences* 37, 51-69.
1184 Kinny, P. D., Williams, I. S., Froude, D. O., Ireland, T. R. & Compston, W. (1988). Early
1185 Archean zircon ages from orthogneisses and anorthosites at Mount Narryer, Western
1186 Australia. *Precambrian Research* 38, 325-341.
1187 Langa, M. M., Jugo, P. J., Leybourne, M. I., Grobler, D. F., Adetunji, J., & Skogby, H. (2020).
1188 Chromite chemistry of a massive chromitite seam in the northern limb of the Bushveld
1189 Igneous Complex, South Africa: correlation with the UG-2 in the eastern and western
1190 limbs and evidence of variable assimilation of footwall rocks. *Mineralium Deposita.*
1191 DOI*:* https://doi.org/10.1007/s00126-020-00964-y.
1192 Lenaz, D. & Princivalle, F. (2005). Crystal chemistry of detrital chromian spinel from the
1193 southeastern Alps and Outer Dinarides: The discrimination of supplies from areas of
1194 similar tectonic setting? *Canadian Mineralogist* 43, 1305-1314.
1195 Lowry, D., Appel, P. W. U., & Rollinson, H. R. (2003). Oxygen isotopes of an early Archean
1196 layered ultramafic body, southern west Greenland: implications for magma source and
1197 post-intrusion history. *Precambrian Research* 126, 273-288.
1198 Marques, A. F. A., Barriga, F. J. A. S. & Scott, S. D. (2007). Sulfide mineralization in an
1199 ultramafic-rock hosted seafloor hydrothermal system: From serpentinization to the
1200 formation of Cu-Zn-(Co)-rich massive sulfides. *Marine Geology* 245, 20-39.

1201 Mondal, S. K., Ripley, E. M., Li, C. & Frei, R. (2006). The genesis of Archaean chromitites
1202 from the Nuasahi and Sukinda massifs in the Singhbhum Craton, India. *Precambrian*
1203 *Research* 148, 45–66.
1204 Mondal, S. K., Ripley, E. M., Li, C., Ahmed, A. H., Arai, S., Liipo, J., & Stowe, C. (2003).
1205 Oxygen isotopic compositions of Cr-spinels from Archean to Phanerozoic chromite
1206 deposits. *Goldschmidt 2003,* 301.
1207 Moore, W. B., & Webb, A. A. G., (2013). Heat-pipe Earth. *Nature* 501, 501-505.
1208 Mukherjee, R., Mondal, S. K., González-Jiménez, J. M., Griffin, W. L., Pearson, N. J. &
1209 O'Reilly, S. Y. (2015). Trace-element fingerprints of chromite, magnetite and sulfides
1210 from the 3.1 Ga ultramafic–mafic rocks of the Nuggihalli greenstone belt, Western
1211 Dharwar craton (India). *Contributions to Mineralogy and Petrology* 169, 59.
1212 Mukherjee, R., Mondal, S. K., Rosing, M. T. & Frei, R. (2010). Compositional variations in the
1213 Mesoarchean chromites of the Nuggihalli schist belt, Western Dharwar Craton (India):
1214 potential parental melts and implications for tectonic setting. *Contributions to*
1215 *Mineralogy and Petrology* 160, 865–885.
1216 Myers, J. S. (1988a). Early Archean Narryer Gneiss Complex, Yilgarn Craton, Western-
1217 Australia. *Precambrian Research* 38, 297-307.
1218 Myers, J. S. (1988b). Oldest known terrestrial anorthosite at Mount Narryer, Western Australia.
1219 *Precambrian Research* 38, 309-323.
1220 Myers, J. S. & Williams, I. R. (1985). Early Precambrian crustal evolution at Mount Narryer,
1221 Western Australia. *Precambrian Research* 27, 153-163.
1222 Nelson, D. R., Robinson, B. W. & Myers, J. S. (2000). Complex geological histories extending
1223 for >= 4.0 Ga deciphered from xenocryst zircon microstructures. *Earth and Planetary*
1224 *Science Letters* 181, 89-102.

1225 Nutman, A. P., Bennett, V. C., Kinny, P. D. & Price, R. (1993). Large-scale crustal structure of
1226 the Northwestern Yilgarn Craton, Western Australia: Evidence from Nd isotopic data
1227 and zircon geochronology. *Tectonics* 12, 971-981.
1228 Nutman, A. P., Kinny, P. D., Compston, W. & Williams, I. S. (1991). SHRIMP U-Pb zircon
1229 geochronology of the Narryer Gneiss Complex, Western Australia. *Precambrian*
1230 *Research* 52, 275-300.
1231 Pidgeon, R. T. & Nemchin, A. A. (2006). High abundance of early Archaean grains and the age
1232 distribution of detrital zircons in a sillimanite-bearing quartzite from Mt Narryer,
1233 Western Australia. *Precambrian Research* 150, 201-220.
1234 Pidgeon, R. T. & Wilde, S. A. (1998). The interpretation of complex zircon U-Pb systems in
1235 Archaean granitoids and gneisses from the Jack Hills, Narryer gneiss Terrane, Western
1236 Australia. *Precambrian Research* 91, 309-332.
1237 Power, M. R., Pirrie, D., Andersen, J. C. Ø., & Wheeler, P. D. (2000). Testing the validity of
1238 chrome spinel chemistry as a provenance and petrogenetic indicator. *Geology* 28 (11),
1239 1027-1030.
1240 Randive, K. R., Korakoppa, M. M., Muley, S. V., Varade, A. M., Khandare, H. W., Lanjewar,
1241 S. G., Tiwari, R. R. & Aradhi, K. K. (2015). Paragenesis of Cr-rich muscovite and
1242 chlorite in green-mica quartzites of Saigaon-Palasgaon area, Western Bastar Craton,
1243 India. *Journal of Earth System Science* 124, 213-225.
1244 Rasmussen, B., Fletcher, I. R., Muhling, J. R., Gregory, C. J. & Wilde, S. A. (2011).
1245 Metamorphic replacement of mineral inclusions in detrital zircon from Jack Hills,
1246 Australia: Implications for the Hadean Earth. *Geology* 39, 1143-1146.
1247 Rasmussen, B., Fletcher, I. R., Muhling, J. R. & Wilde, S. A. (2010). In situ U-Th-Pb
1248 geochronology of monazite and xenotime from the Jack Hills belt: Implications for the

1249 age of deposition and metamorphism of Hadean zircons. *Precambrian Research* 180,
1250 26-46.
1251 Rollinson, H., Reid, C., & Windley, B. (2010). Chromitites from the Fiskenæsset anorthositic
1252 complex, West Greenland: clues to late Archaean mantle processes. In: Kusky, T. M.,
1253 Zhai, M.-G. & Xiao, W. (eds) *The Evolving Continents: Understanding Processes of*
1254 *Continental Growth:* Geological Society, London, Special Publications, 338, 197–212.
1255 Rollinson, H., Appel, P. W. U. & Frei, R. (2002). A metamorphosed, early Archaean chromitite
1256 from west Greenland: Implications for the genesis of Archaean anorthositic chromitites.
1257 *Journal of Petrology* 43, 2143-2170.
1258 Rowe, M. L., & Kemp, A. I. S. (2020). Spinel, olivine, and pyroxene chemistry of the
1259 Eoarchaean Manfred Complex (Yilgarn Craton, Western Australia), with implications
1260 for the tectonic setting of Archaean layered mafic intrusions and the stabilisation of
1261 continental nuclei. *Lithos* 356-357. DOI: 10.1016/j.lithos.2019.105340.
1262 Rozel, A., Golabek, G., Jain, C., Tackley, P. & Gerya, T. (2017). Continental crust formation
1263 on early Earth controlled by intrusive magmatism. *Nature* 545, 332-338.
1264 Santti, J., Kontinen, A., Sorjonen-Ward, P., Johanson, B. & Pakkanen, L. (2006).
1265 Metamorphism and chromite in serpentinized and carbonate-silica-altered peridotites of
1266 the Paleoproterozoic Outokumpu-Jormua ophiolite belt, eastern Finland. *International*
1267 *Geology Review* 48, 494-546.
1268 Schannor, M., Veksler, I. V., Hecht, L., Harris, C., Romer, R. L., & Manyeruke, T. D. (2018).
1269 Small-scale Sr and O isotope variations through the UG2 in the eastern Bushveld
1270 Complex: The role of crustal fluids. *Chemical Geology* 485, 100-112.
1271 Shirey, S. B. & Walker, R. J. (1998). The Re-Os isotope system in cosmochemistry and high-
1272 temperature geochemistry. *Annual Review of Earth and Planetary Sciences* 26, 423-
1273 500.

1274 Spaggiari, C. V. (2007a). Structural and lithological evolution of the Jack Hills greenstone belt,
1275 Narryer Terrane, Yilgarn Craton, Western Australia. *Western Australia Geological*
1276 *Survey* Record 2007/3, 49.
1277 Spaggiari, C. V., Pidgeon, R. T. & Wilde, S. A. (2007b). The Jack Hills greenstone belt,
1278 Western Australia - Part 2: Lithological relationships and implications for the deposition
1279 of > 4.0 Ga detrital zircons. *Precambrian Research* 155, 261-286.
1280 Szilas, K., van Hinsberg, V., McDonald, I., Naeraa, T., Rollinson, H., Adetunji, J. & Bird, D.
1281 (2018). Highly refractory Archaean peridotite cumulates: Petrology and geochemistry
1282 of the Seqi Ultramafic Complex, SW Greenland. *Geoscience Frontiers* 9, 689-714.
1283 Tang, M., Chen, K. & Rudnick, R. (2016). Archean upper crust transition from mafic to felsic
1284 marks the onset of plate tectonics. *Science* 351, 372-375.
1285 Tarduno, J. A., Cottrell, R. D., Bono, R. K., Oda, H., Davis, W. J., Fayek, M., van't Erve, O.,
1286 Nimmo, F., Huang, W., Thern, E. R., Fearn, S., Mitra, G., Smirnov, A. V., & Blackman,
1287 E. G. (2020). Paleomagnetism indicates that primary magnetite in zircon records a
1288 strong Hadean geodynamo. *Proceedings of the National Academy of Sciences of the*
1289 *United States of America* 117 (5), 2309-2318.
1290 Valley, J. W., Cavosie, A. J., Ushikubo, T., Reinhard, D. A., Lawrence, D. F., Larson, D. J.,
1291 Clifton, P. H., Kelly, T. F., Wilde, S. A., Moser, D. E. & Spicuzza, M. J. (2014). Hadean
1292 age for a post-magma-ocean zircon confirmed by atom-probe tomography. *Nature*
1293 *Geoscience* 7, 219-223.
1294 Valley, J. W., Cavosie, A. J., Shirey, S. & Wilde, S. A. (2005). 3.2 to 3.5 Ga Re-Os Model Ages
1295 for Detrital Chromite from Jack Hills, Western Australia: Implications for Pilbara and
1296 Yilgarn Craton Evolution. *American Geophysical Union, Fall Meeting 2005, abstract*
1297 *#V21F-08*.
1298 Valley, J., Peck, W., King, E. & Wilde, S. (2002). A cool early Earth. *Geology* 30, 351-354.

1299 Valley, J. W., Kitchen, N., Kohn, M., Niendorf, C. R., & Spicuzza, M. J. (1995). UWG-2, a
1300 garnet standard for oxygen isotope ratios: strategies for high precision and accuracy
1301 with laser heating. *Geochimica et Cosmochimica Acta* 59, 5223– 5231.
1302 Van Baalen, M. (1993). Titanium mobility in metamorphic systems - a review. *Chemical*
1303 *Geology* 110, 233-249.
1304 Wang, Q. & Wilde, S. A. (2018). New constraints on the Hadean to Proterozoic history of the
1305 Jack Hills belt, Western Australia. *Gondwana Research* 55, 74-91.
1306 Wilde, S. A., Valley, J. W., Peck, W. H. & Graham, C. M. (2001). Evidence from detrital
1307 zircons for the existence of continental crust and oceans on the Earth 4.4 Gyr ago.
1308 *Nature* 409, 175-178.
1309 Williams, I. R. & Myers, J. S. (1987). Archaean geology of the Mount Narryer region Western
1310 Australia. Geological Survey of Western Australia: Report 22, 1-32.
1311 Wood, B. J. & Virgo, D. (1989). Upper mantle oxidation-state: ferric iron contents of lherzolite
1312 spinels by Fe-57 Mossbauer-spectroscopy and resultant oxygen fugacities. *Geochimica*
1313 *et Cosmochimica Acta* 53, 1277-1291.
1314 Wyche, S. (2007). Evidence of Pre-3100 Ma Crust in the Youanmi and South West Terranes,
1315 and Eastern Goldfields Superterrane, of the Yilgarn Craton. In: van Kranendonk, M. J.,
1316 Smithies, R. H. & Bennett, V. C. (eds.) *Earth's Oldest Rocks*: Elsevier, 113-124.
1317 Wyche, S., Nelson, D. R. & Riganti, A. (2004). 4350-3130 Ma detrital zircons in the Southern
1318 Cross Granite-Greenstone Terrane, Western Australia: Implications for the early
1319 evolution of the Yilgarn Craton. *Australian Journal of Earth Sciences* 51, 31-45.
1320 Wylie, A. G., Candela, P. A. & Burke, T. M. (1987). Compositional zoning in unusual Zn-rich
1321 chromite from the Sykesville District of Maryland and its bearing on the origin of
1322 ferritchromit. *American Mineralogist* 72, 413-422.

1323 Zheng, Y. -F. (1991). Calculation of oxygen isotope fractionation in metal oxides.

1324 *Geochimica et Cosmochimica Acta* 55, 2299-2307.

1325

1326 Detrital chromite from Jack Hills, Western Australia: signatures of metamorphism and
1327 constraints on chromite provenance
1328
1329 Figure captions
1330
1331 Fig. 1: Map of the Yilgarn Craton, Western Australia, showing the position of the Narryer
1332 Terrane, Jack Hills and Mount Narryer. Modified from Kemp et al., 2018 with Terrane
1333 boundaries after Cassidy *et al.* (2006).
1334
1335 Fig. 2: (a) Simplified geological map of Jack Hills and surrounding quartzofeldspathic gneiss
1336 and granitoids with sampling locations, after Spaggiari *et al.* (2007b) and Pidgeon & Wilde
1337 (1998). (b) Higher resolution geological map of sampling locations at and around the W-74
1338 discovery site (see Fig. 2a). Modified after Spaggiari *et al.* (2007b). See Methods and Materials
1339 for relative positions of samples from the W-74 site.
1340
1341 Fig. 3: Jack Hills detrital chromite. (a) Optical microscope image illustrating e*x-situ* variably
1342 rounded morphologies of chromite grains. Note the green-brown fuchsite. (b) BSE image of
1343 chromite observed *in-situ* within quartzite cobble. Despite isolation from metaconglomerate
1344 matrix the cobble has been infiltrated by secondary Cr-muscovite. (c) BSE image of complex
1345 and ragged boundaries between chromite and fuchsite within metaconglomerate matrix. Grain
1346 heavily fractured on its southern margin. Chr – chromite, Qz – quartz, Fch – fuchsite. Iron
1347 oxides are likely magnetite, but have not been analysed by EPMA.
1348

Fig. 4: BSE images showing chromite textural variation. All scale bars 50 μm. (a) Smooth with minimal fracturing, commonly associated with high Cr#. (b) Polygonal fracturing, no pitted domains. (c) Fractured with very fine pitted domains. Note coarser pores, with pitted domains localised to edges and near fractures. (d) Fractured with increasingly pitted textures, often away from obvious fractures. (e) and (f) porous chromite, fractures apparently lost or in-filled by secondary material. Secondary material often aligned to crystallographic axes. Qz – quartz, Fch – fuchsite and Rt- rutile. Iron oxides are likely magnetite, but have not been analysed by EPMA.

Fig. 5: BSE images of inclusion assemblages. (a) Isolated euh-subhedral quartz (Qz). Brighter crystallites in quartz are rutile, an Mg-silicate, and phosphate. Note the surrounding pitted domain, including darker quartz and rutile (Rt) laths, but absence of cracks. (b) Isolated polyphase assemblage of quartz and iron oxide. (c) Subhedral Fe-sulphide within pitted domain of chromite; pyrrhotite (Po) and chalcopyrite (Ccp) (outlined in red). (d) Euhedral rutile within quartz; note the ragged boundaries of quartz and surrounding pitted domain. (e) Anhedral inclusion of fuchsite. (f) Globular inclusion of quartz and fuchsite with monazite. Note the expansion cracks radiating from inclusion.

Fig. 6: Variation of Mg#, ZnO, MnO and TiO_2. Each data point is separated by sample and represents a core or near-core composition of chromite. Slightly elevated Mg# of 01JH chromites in comparison to those from 14WA and 16WA is a function of higher ferric iron contents. (a) ZnO vs Mg#. (b) MnO vs Mg#. (c) TiO_2 vs Mg#. Most grains yield low TiO_2 of <0.25 wt.%. It is likely that some analyses above this value overlapped with subsurface rutile laths. However, some grains with >0.25 wt.% TiO_2 show no evidence of rutile laths. TiO_2 >1 wt.% clearly represent overlap with rutile laths, so are omitted. (d) MnO vs ZnO.

Fig. 7: Variation of Cr#. (a) ZnO vs Cr#. No variation in the range of Cr# despite apparent increasing ZnO. (b) Cr# vs Fe^{2+}# (100x molar $Fe^{2+}/(Fe^{2+}+Fe^{3+})$). (c) TiO_2 concentrations vs Cr#. Scatter towards 1 wt.% a mixture of high TiO_2 grains and likely overlap of rutile laths. High Cr# grains appear to be slightly elevated in TiO_2 in comparison to bulk lower Cr# grains. (d) $Fe^{3+}/\Sigma Fe$ vs Cr#. Significant non-stoichiometry of 14WA and 16WA chromites has resulted in markedly lower $Fe^{3+}/\Sigma Fe$ in comparison to 01JH chromites.

Fig. 8: Examples of zonation patterns observed within 14WA and 16WA Jack Hills detrital chromites, including BSE images of line path taken. Isolated, globular inclusions of fuchsite (fch) also highlighted in 14WA2-PB-46. (a) Decreasing Mg# towards rims: most commonly shown by low ZnO samples 14WA2 and 16WA5. 14WA2-PB-46 yields the most variable zoning patterns observed in all Jack Hills grains and is likely the least altered grain analysed. This example also includes elevated Fe_2O_3 at its rims, resulting in an area of slightly elevated Cr#. (b) Elevated Mg# towards rims: commonly observed in high ZnO samples such as 14WA3-4 and 16WA7. ZnO and Mn are lost from chromite at the expense of FeO and MgO, increasing the Mg# of rims relative to the core of the grain. (c) Largely homogeneous Mg#. No change in mineral chemistry across the grain in divalent or trivalent cations; this example has a slight elevation in Mg# on one edge after a minor decrease from the core.

Fig. 9: Variation in mineral chemistry: BSE images with elevated contrast to variable high Cr# domains. (a) and (b) High Cr#, pit-free domains at the edge of grains, and (c) along or associated with cracks. (d) and (e) High Cr# domains bound by chromite crystallographic axes, closely associated with laths of fuchsite (fch) and anhedral quartz (qz) along margins of high Cr# zones

and rutile (rt). (f) The only observed example of a domain of lowered Cr#, encircling an inclusion of quartz with iron oxide rims. Note the radial fractures associated with the secondary inclusion. Except where stated, all scale bars are 50 μm.

Fig.10: Oxygen isotope ratios ($\delta^{18}O$ reported at ‰ variation to V-SMOW) for different size fractions of Jack Hills detrital chromite grains measured by laser fluorination. $\delta^{18}O$ uncertainties (2σ) are ±0.08 for 01JH36, ± 0.12 for 01JJ42 and ±0.06 for 01JH54. (a) and (b) Samples 01JH36 and 01JH42, which show strong evidence of grain size dependency on $\delta^{18}O$ values. (c) Sample 01JH54, showing no evidence of grain size dependency on $\delta^{18}O$ values.

Fig. 12: Cr^{3+}-Al^{3+}-Fe^{3+} triangular plot, modified from Barnes & Roeder (2001), showing three magmatic compositional pathways for spinel: Cr-Al, Fe-Ti, and Rum trends. The compositional space of ferritchromit, Cr-magnetite, and spinel miscibility gaps shown for reference. Core or near core compositions of low ZnO 14WA2 and 01JH54 chromites are shown.

Fig. 12: Provenance: Cr# vs Fe^{2+}# ($100xFe^{2+}/(Fe^{2+}+Mg2^{+})$, diagrams modified from Barnes & Roeder (2001). (a) Strong fit of 14WA2 detrital chromite with chromite that have undergone high-grade metamorphism due to exchange of Mg^{2+} for Fe^{2+}, and thus increased Fe^{2+}#. (b) Fit of bulk field for chromite from ophiolites, although Jack Hills chromites plot at considerably higher Fe^{2+}# due to metamorphic exchange of Mg^{2+} for Fe^{2+}. (c) Strong fit of chromite Cr# in Jack Hills chromite with chromite from continental layered mafic intrusions. Jack Hills detrital chromite Fe^{2+}# are again largely higher than 50^{th} percentile due to metamorphic exchange. (d)

Distinct absence of fit with chromite from Al-undepleted (AUD) komatiites. GSF; Greenschist facies AUD komatiites, AF; Amphibolite facies AUD komatiites.

Fig. 13: Provenance: TiO_2 vs. $Fe^{3+}/\Sigma R^{3+}$, diagrams modified from Barnes & Roeder (2001). Chromites that ostensibly yield no Fe^{3+} from 14WA2 are excluded for clarity. Fit of 14WA2 and 01JH54 chromite to all fields for and (a) ophiolites, (b) layered intrusions and (c) Al-undepleted komatiites. GSF; Greenschist facies komatiites, AF; Amphibolite facies komatiites.

Fig. 14: Cr-spinel compositions from the Narryer Terrane. BSE images of Manfred Complex 13TKN22 chromite; (a) finer chromite (chr) within 13TKN22, with a strong magnetite rim (mag) and an inclusion of olivine (ol), and (b) coarser chromite within hornblende (hbl). Serpentine (srp) and magnetite (mag) also shown. (c) and (d) Relict, porous chromite with thick ferritchromit and magnetite rims within 16WA13, an ultramafic from the SW limb of the Jack Hills belt. Note the softening of the boundary between core and rim in comparison to 13TKN22. (e)-(g) Compositional variability of 13TKN22 and 16WA13 chromite in comparison to Jack Hills detrital chromites. Spinel compositional fields from Manfred Complex harzburgites and websterites reported by Rowe & Kemp (2020) included for comparison. Layered intrusion fields from Barnes & Roeder (2001). (e) Cr^{3+}-Al^{3+}-Fe^{3+} triangular plot, (f) Cr# vs Fe^{2+}# and (g) TiO_2 vs $Fe^{3+}/\Sigma R^{3+}$.

Fig. 15: The inferred petrogenesis of Jack Hills chromites. (a) Original igneous crystallisation in a single, spatially extensive igneous protolith, postulated to represent a layered intrusion. (b) Exhumation of layered intrusion and first sedimentary cycling event. Continued erosion

resulted in loss of contemporaneous silicates; some chromites preserved isolated within quartzite. Chromites (±zircon) now observed within the matrix of Jack Hills metasedimentary rocks present previously in heavy mineral layers or disseminated throughout quartzite. (c) Further sedimentary reworking in second cycling event deposits chromites in Jack Hills conglomerates and quartzites. Dispersion of chromites and zircons within both quartzite cobbles and matrix. (d) Metamorphism of Jack Hills metasedimentary rocks at ~2650 Ma, likely representing peak metamorphism at upper greenschist to lower amphibolite facies. This event also formed fuchsite and other metamorphic assemblages within the host metasedimentary rock, replaced chromite primary inclusion assemblages, and led to the partial to complete exchange of chromite divalent cations with metamorphic fluids. (e) Proterozoic metamorphic overprint of metasediments within the Jack Hills. Minor metamorphic exchange potentially indicated by zonation profiles.

Fig.1

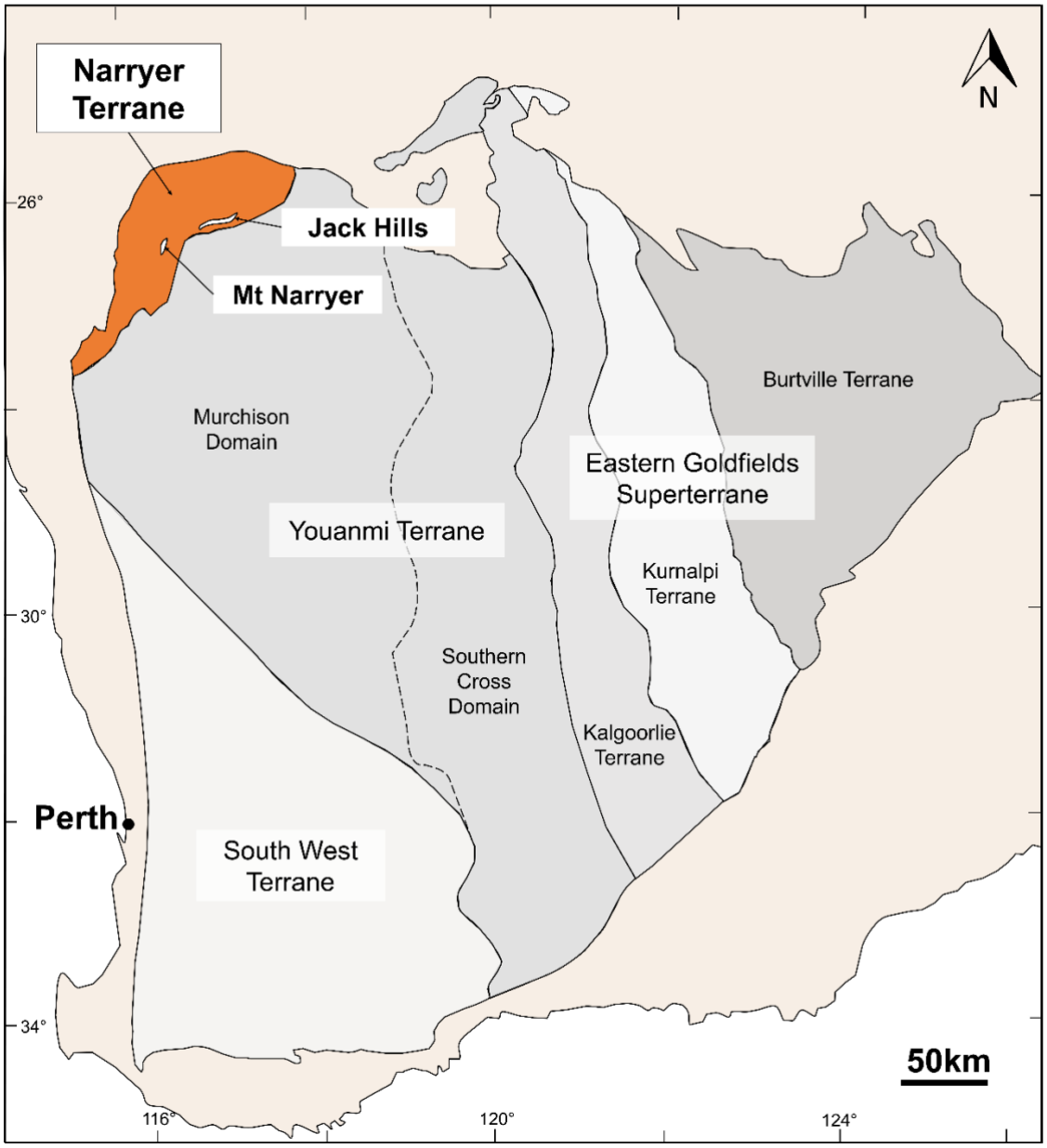
Narryer Terrane
Jack Hills
Mt Narryer
N
26°
Murchison Domain
Youanmi Terrane
Eastern Goldfields Superterrane
Burtville Terrane
Kurnalpi Terrane
Southern Cross Domain
Kalgoorlie Terrane
30°
Perth
South West Terrane
34°
50km
116°
120°
124°

Fig.2

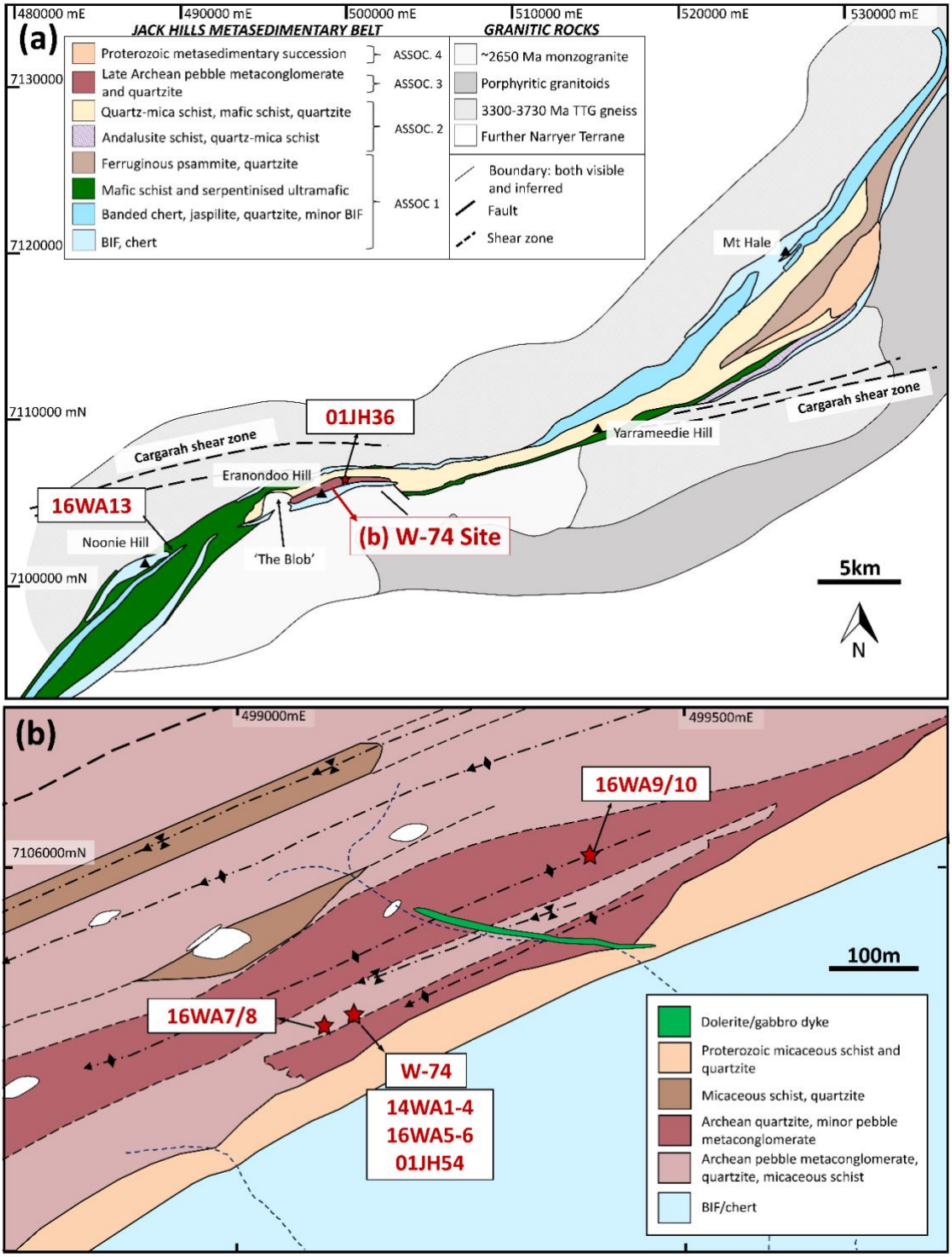

To add: **01JH35 sampling location**

Fig. 3

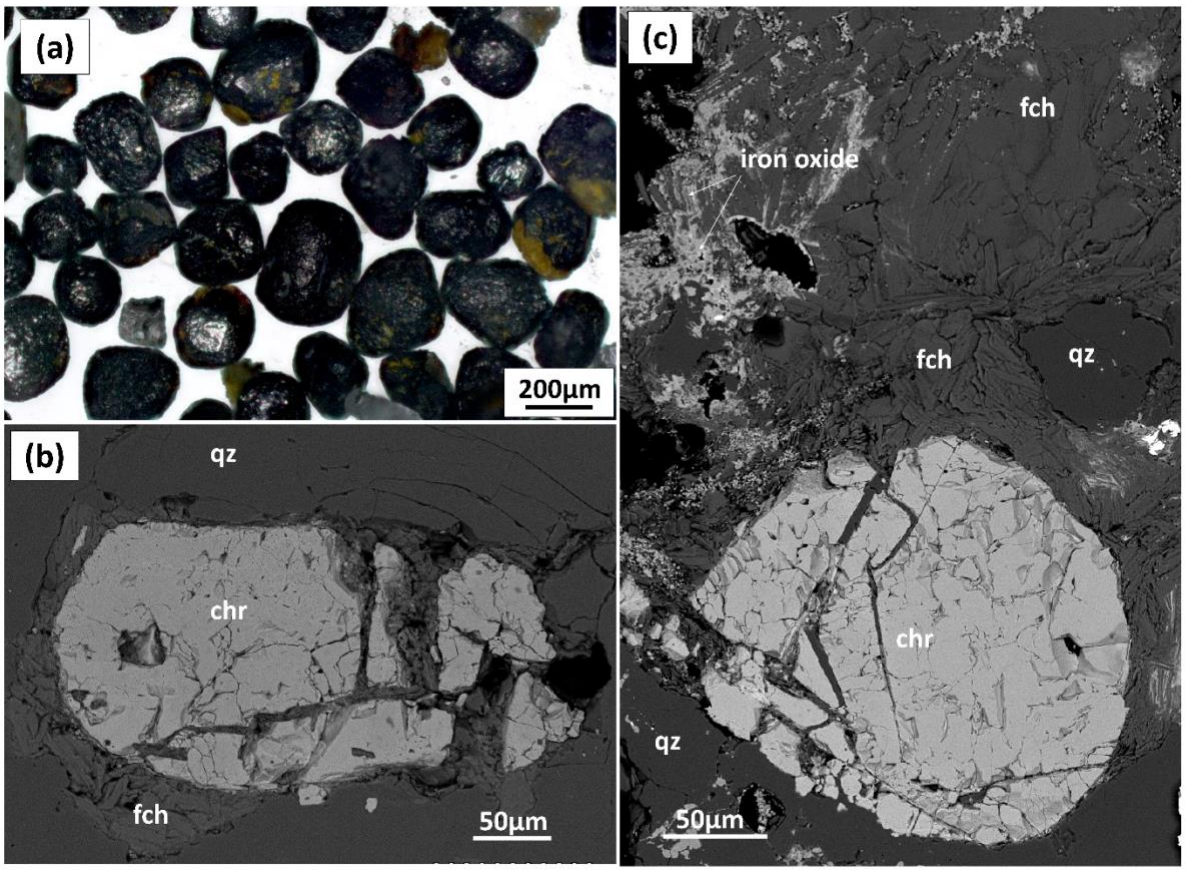

Fig. 4

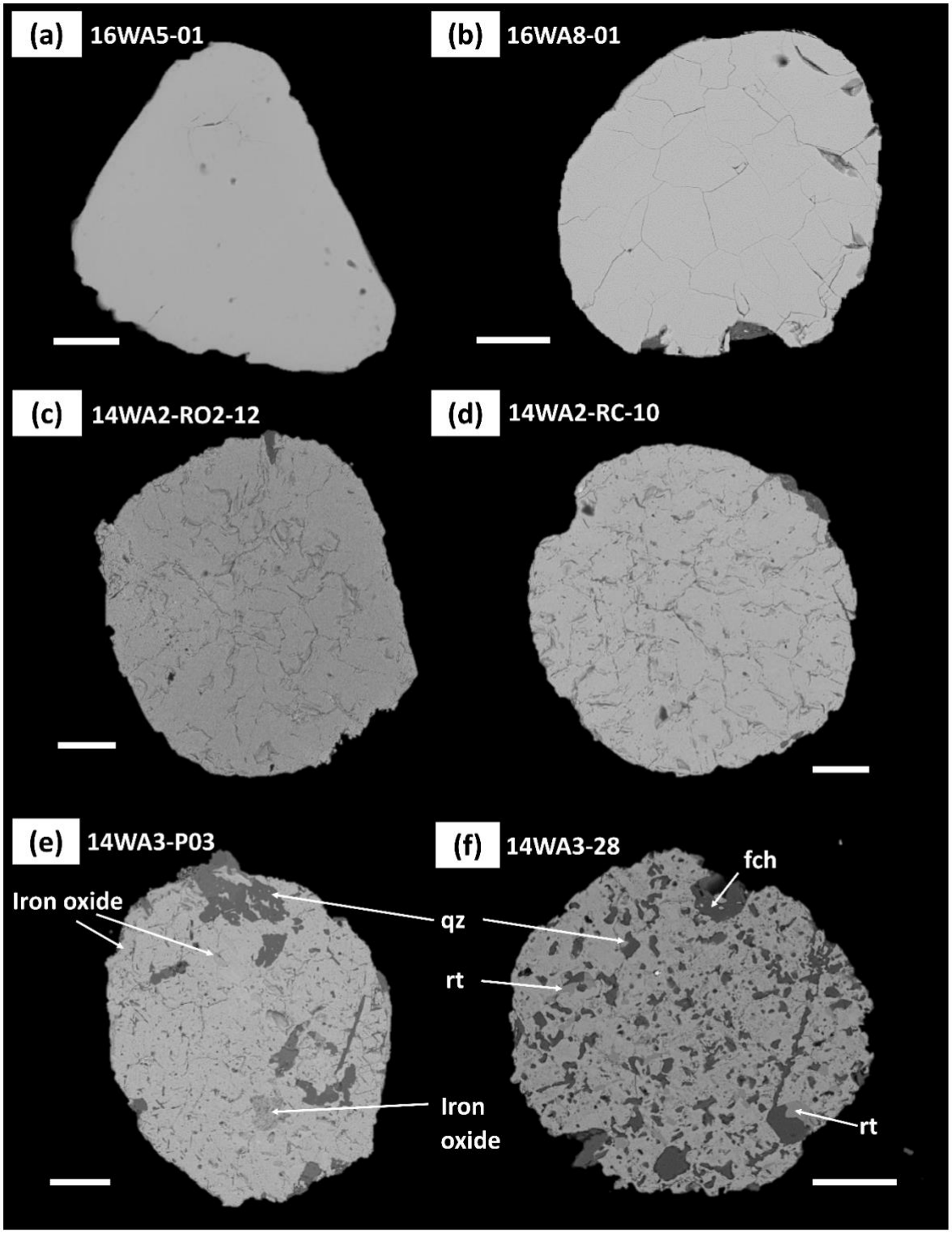
(a) 16WA5-01
(b) 16WA8-01
(c) 14WA2-RO2-12
(d) 14WA2-RC-10
(e) 14WA3-P03
Iron oxide
qz
Iron oxide
(f) 14WA3-28
fch
rt
rt

Fig. 5

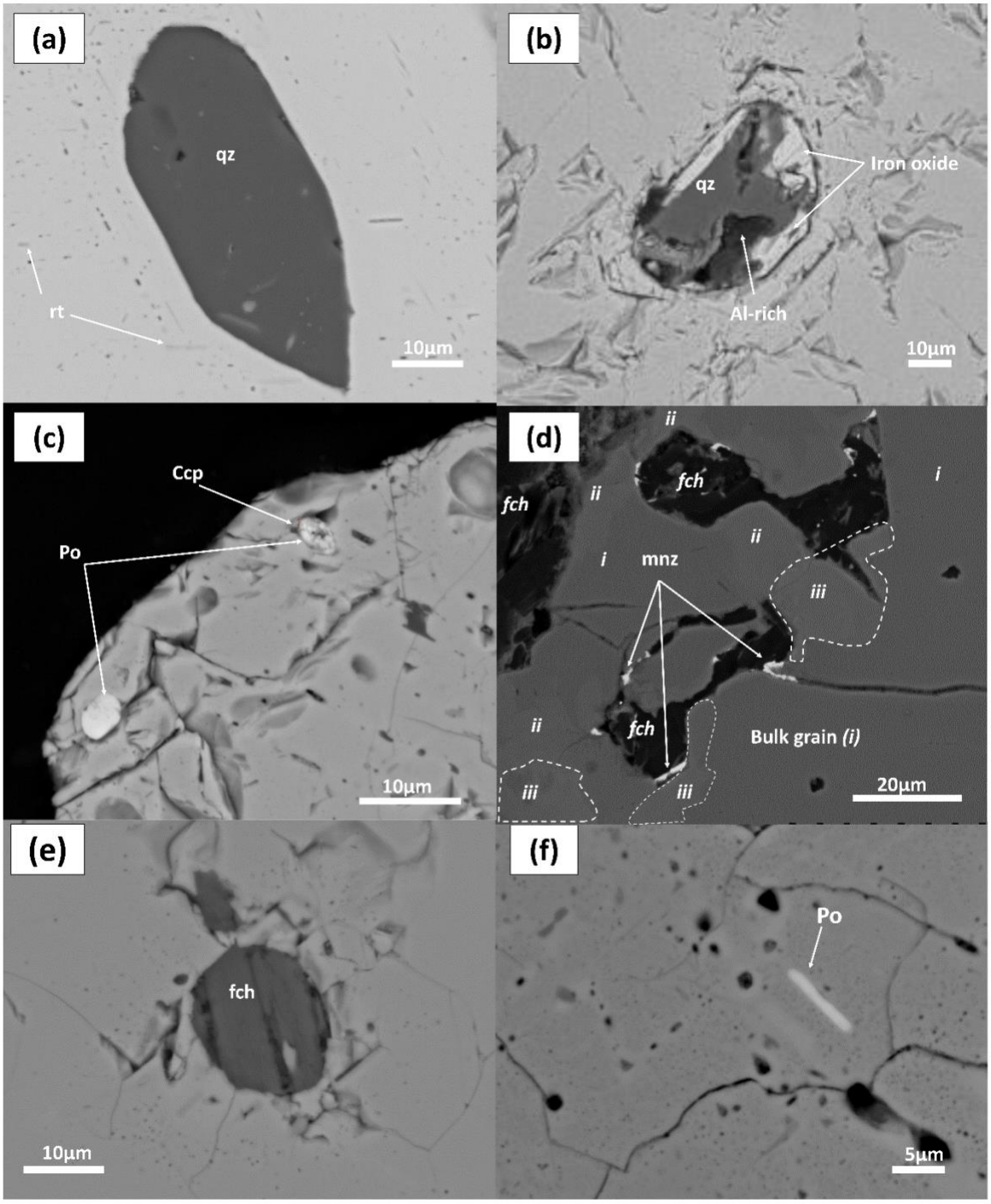
(a)
qz
rt
10µm
(b)
qz
Iron oxide
Al-rich
10µm
(c)
Ccp
Po
10µm
(d)
ii
fch
i
fch
ii
ii
i
mnz
iii
ii
fch
Bulk grain (i)
iii
iii
20µm
(e)
fch
10µm
(f)
Po
5µm

Fig. 6

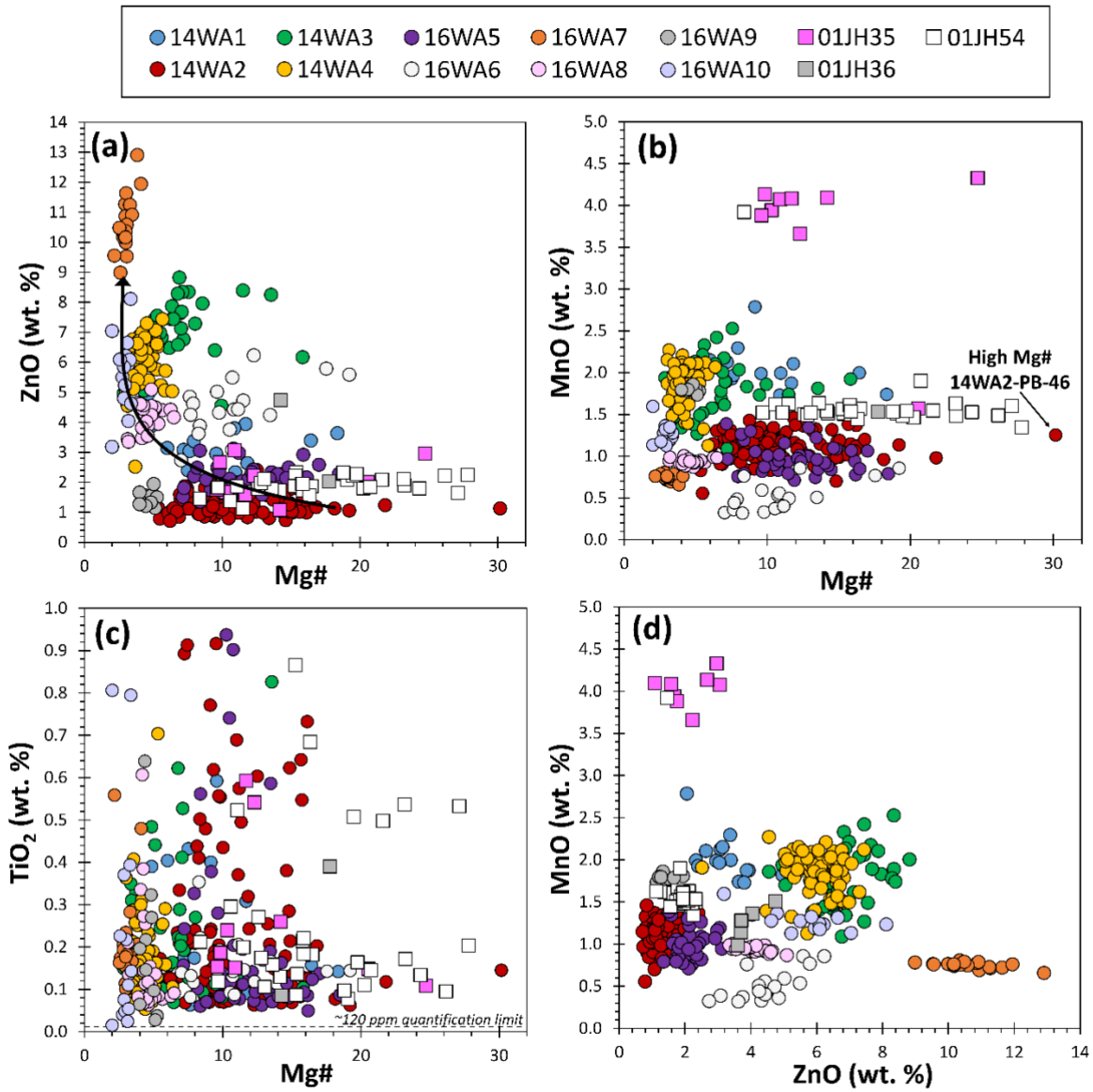
14WA1
14WA2
14WA3
14WA4
16WA5
16WA6
16WA7
16WA8
16WA9
16WA10
01JH35
01JH36
01JH54
(a)
ZnO (wt. %)
Mg#
(b)
MnO (wt. %)
High Mg#
14WA2-PB-46
Mg#
(c)
TiO2 (wt. %)
~120 ppm quantification limit
Mg#
(d)
MnO (wt. %)
ZnO (wt. %)

Fig. 7

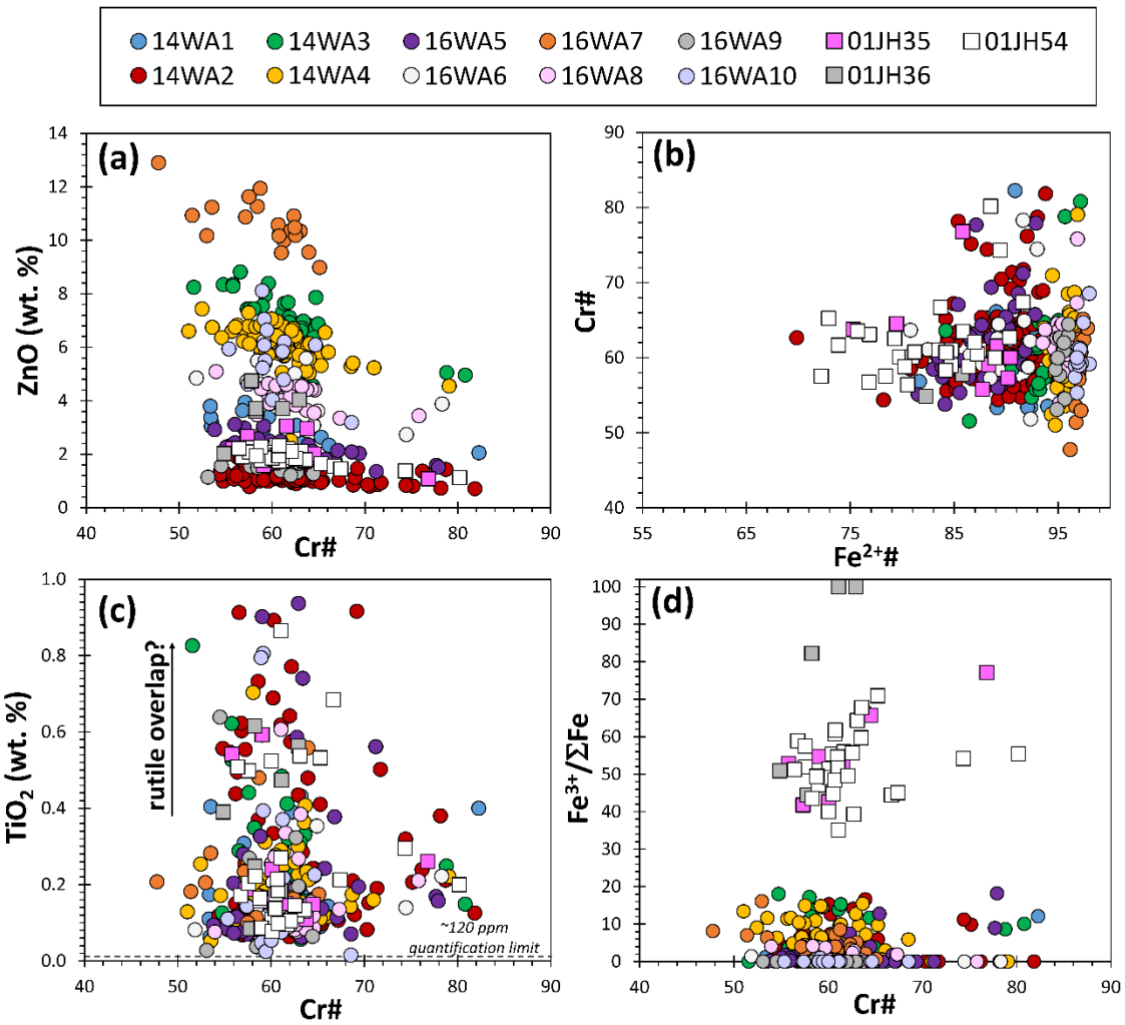
14WA1
14WA2
14WA3
14WA4
16WA5
16WA6
16WA7
16WA8
16WA9
16WA10
01JH35
01JH36
01JH54
(a)
ZnO (wt. %)
Cr#
(b)
Cr#
Fe2+#
(c)
TiO2 (wt. %)
rutile overlap?
~120 ppm
quantification limit
Cr#
(d)
Fe3+/∑Fe
Cr#

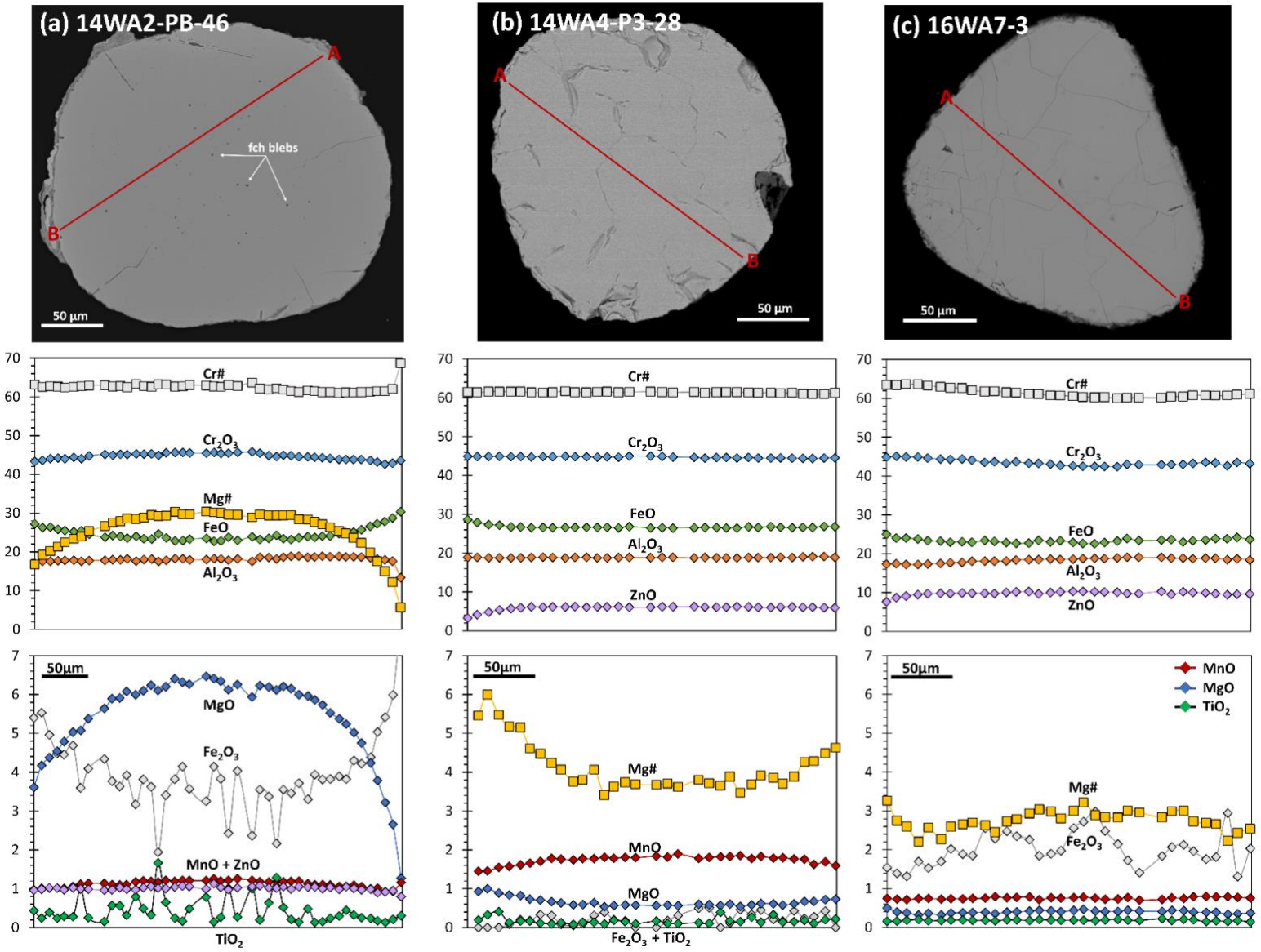
(a) 14WA2-PB-46
A
B
fch blebs
50 µm
(b) 14WA4-P3-28
A
B
50 µm
(c) 16WA7-3
A
B
50 µm
Cr#
Cr2O3
Mg#
FeO
Al2O3
FeO
Al2O3
ZnO
MgO
Fe2O3
MnO + ZnO
TiO2
MnO
Mg#
Fe2O3 + TiO2
MgO
TiO2

Fig. 8

Fig. 9

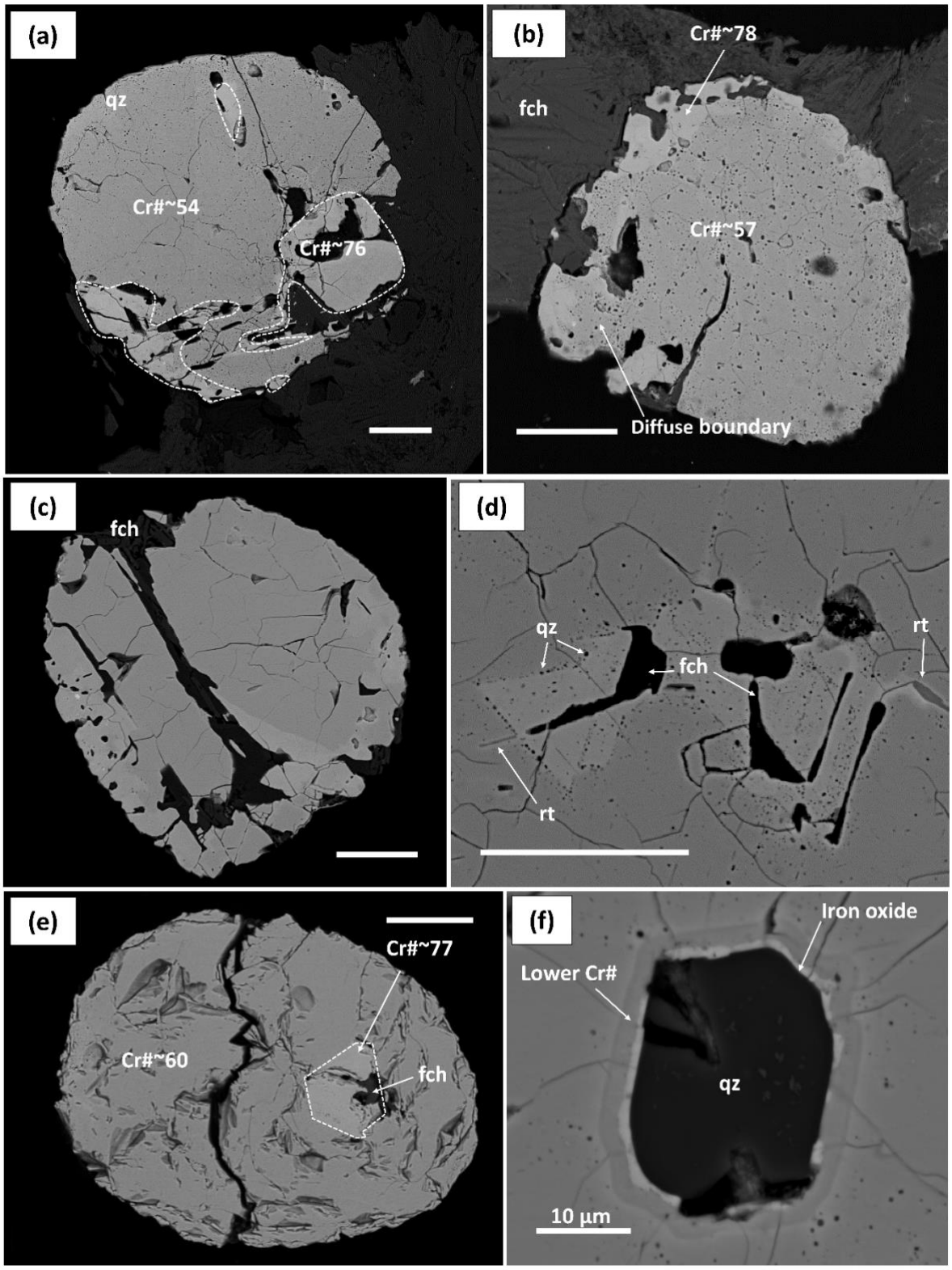
(a)
qz
Cr#~54
Cr#~76
(b)
Cr#~78
fch
Cr#~57
Diffuse boundary
(c)
fch
(d)
qz
fch
rt
rt
(e)
Cr#~77
Cr#~60
fch
(f)
Iron oxide
Lower Cr#
qz
10 µm

Fig. 10

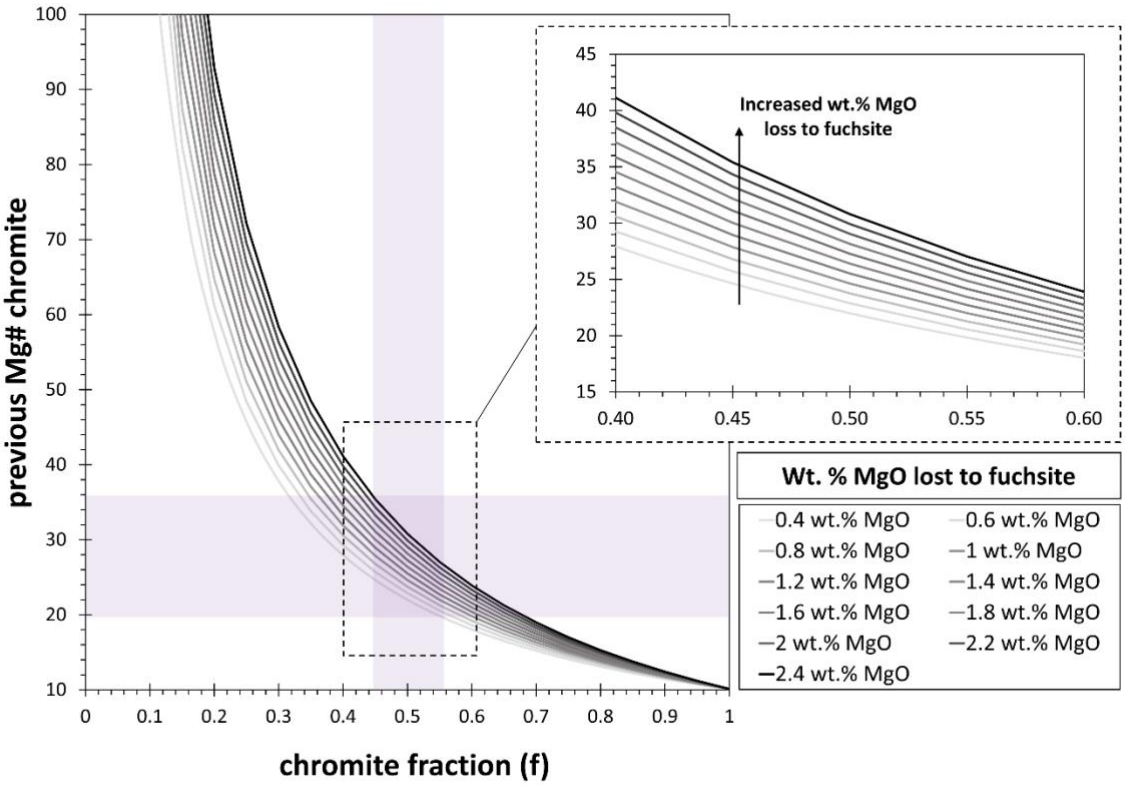
previous Mg# chromite
chromite fraction (f)
Increased wt.% MgO loss to fuchsite
Wt. % MgO lost to fuchsite
0.4 wt.% MgO
0.6 wt.% MgO
0.8 wt.% MgO
1 wt.% MgO
1.2 wt.% MgO
1.4 wt.% MgO
1.6 wt.% MgO
1.8 wt.% MgO
2 wt.% MgO
2.2 wt.% MgO
2.4 wt.% MgO

Fig. 11

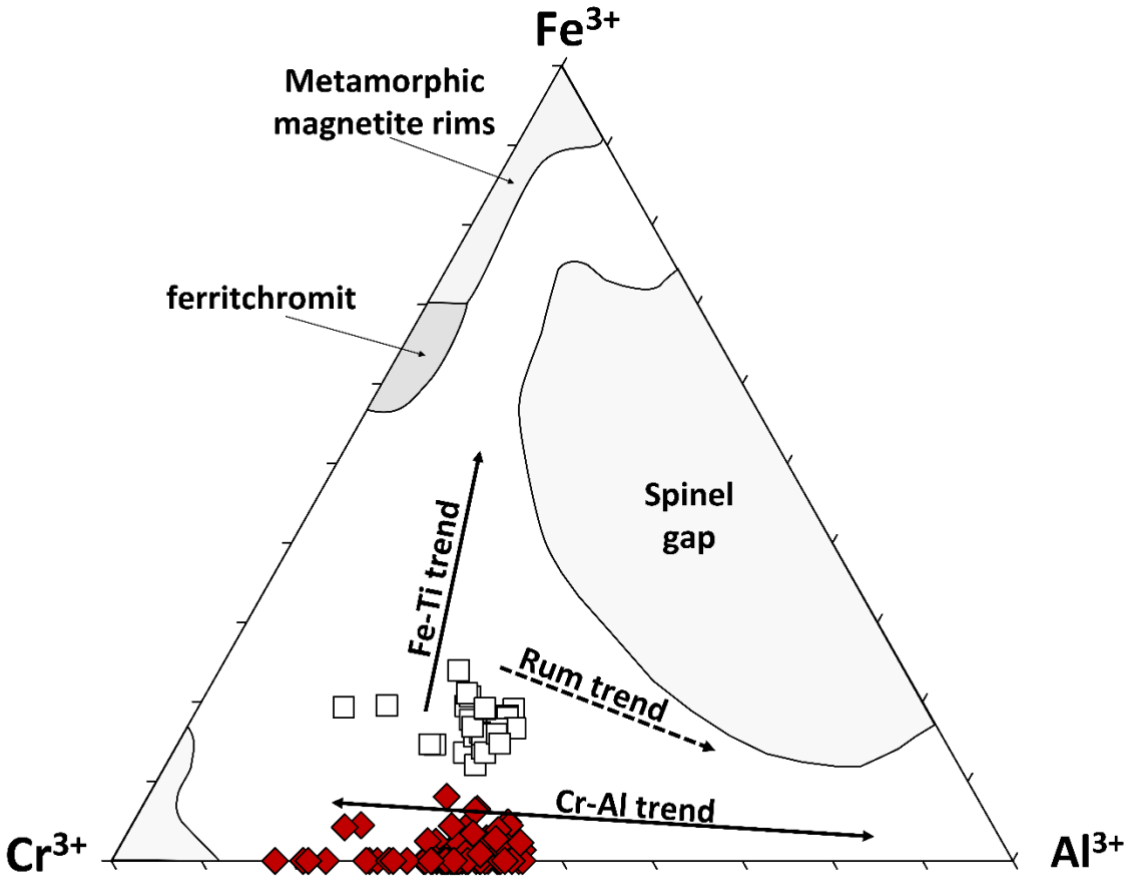
Fe3+
Metamorphic
magnetite rims
ferritchromit
Spinel
gap
Fe-Ti trend
Rum trend
Cr-Al trend
Cr3+
Al3+

Fig. 12

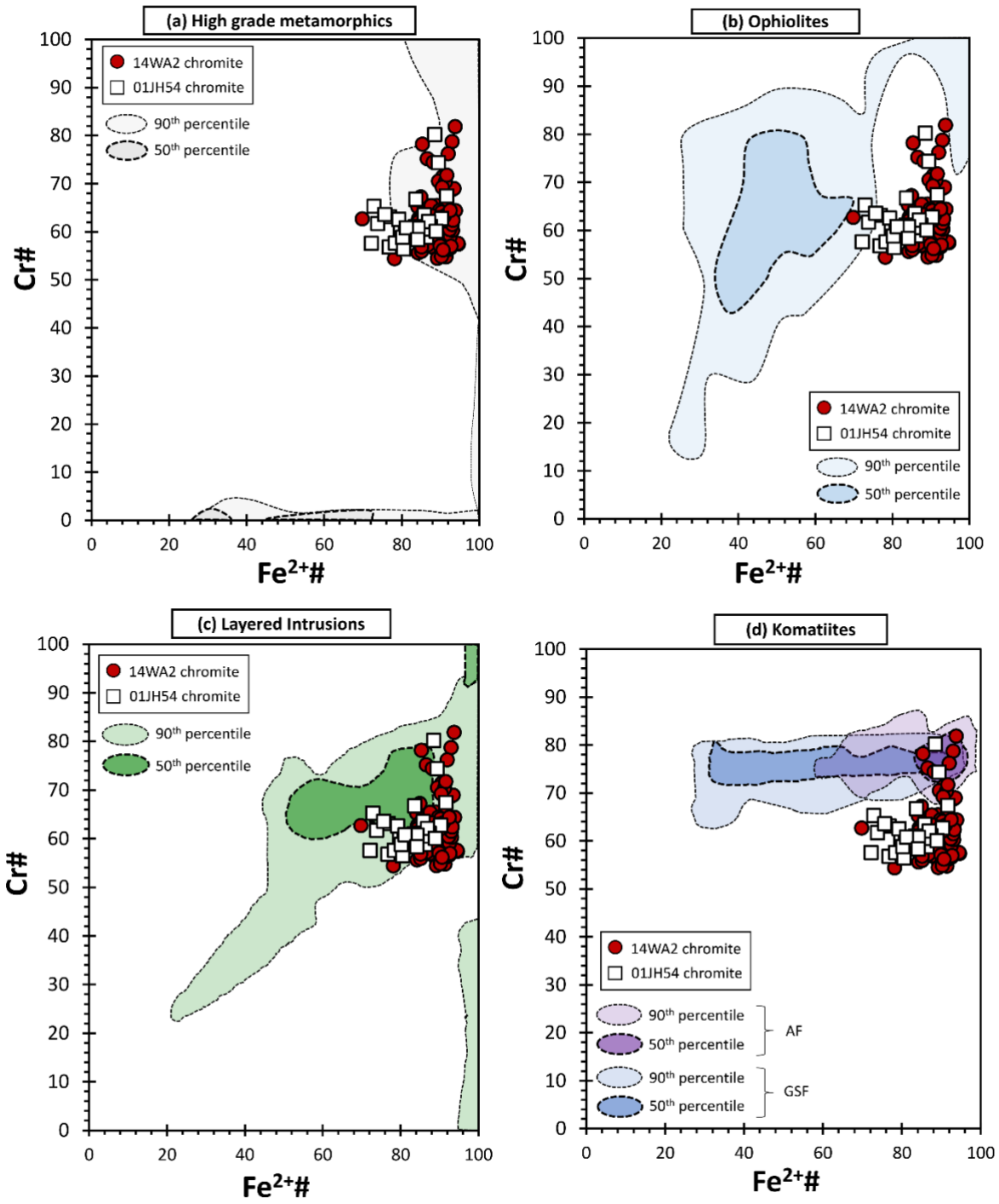
(a) High grade metamorphics
(b) Ophiolites
(c) Layered Intrusions
(d) Komatiites
14WA2 chromite
01JH54 chromite
90th percentile
50th percentile
AF
GSF
Cr#
Fe2+#

Fig. 13

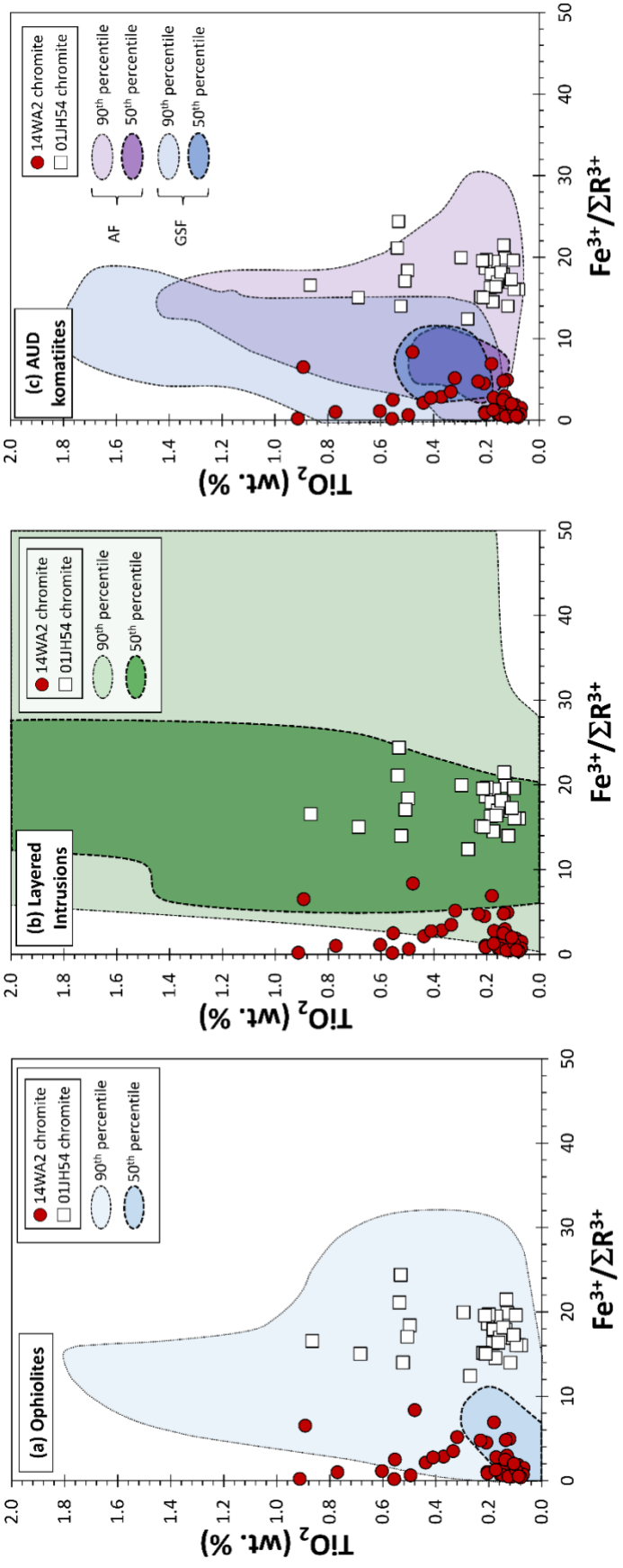
(a) Ophiolites
(b) Layered Intrusions
(c) AUD komatiites
14WA2 chromite
01JH54 chromite
90th percentile
50th percentile
AF
GSF
TiO2 (wt. %)
Fe3+/∑R3+

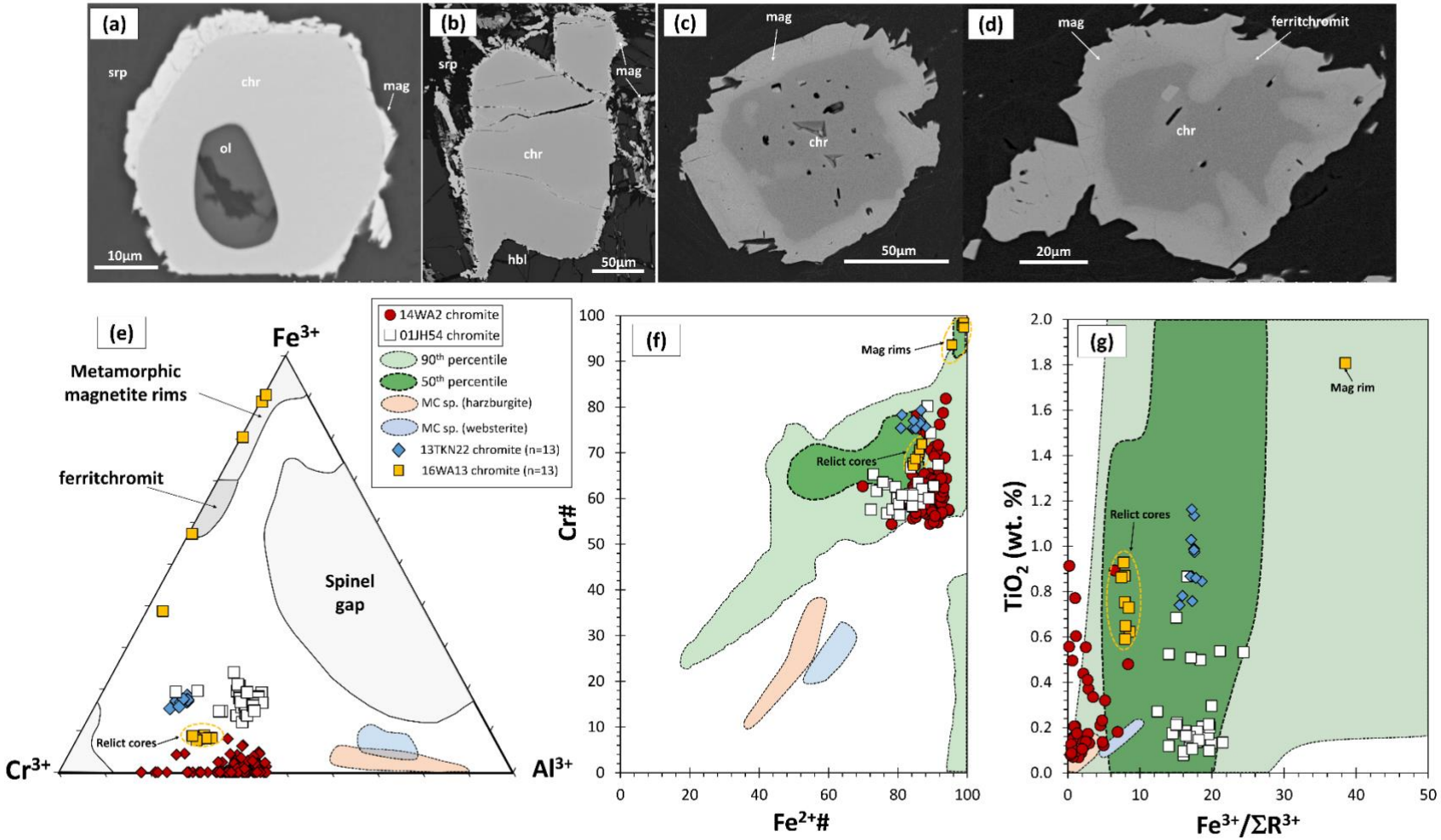
(a)
srp
chr
mag
ol
10µm
(b)
srp
mag
chr
hbl
50µm
(c)
mag
chr
50µm
(d)
mag
ferritchromit
chr
20µm
(e)
Fe3+
Metamorphic magnetite rims
ferritchromit
Spinel gap
Relict cores
Cr3+
Al3+
14WA2 chromite
01JH54 chromite
90th percentile
50th percentile
MC sp. (harzburgite)
MC sp. (websterite)
13TKN22 chromite (n=13)
16WA13 chromite (n=13)
(f)
Mag rims
Relict cores
Cr#
Fe2+#
(g)
Mag rim
Relict cores
TiO2 (wt. %)
Fe3+/ΣR3+

Fig. 14

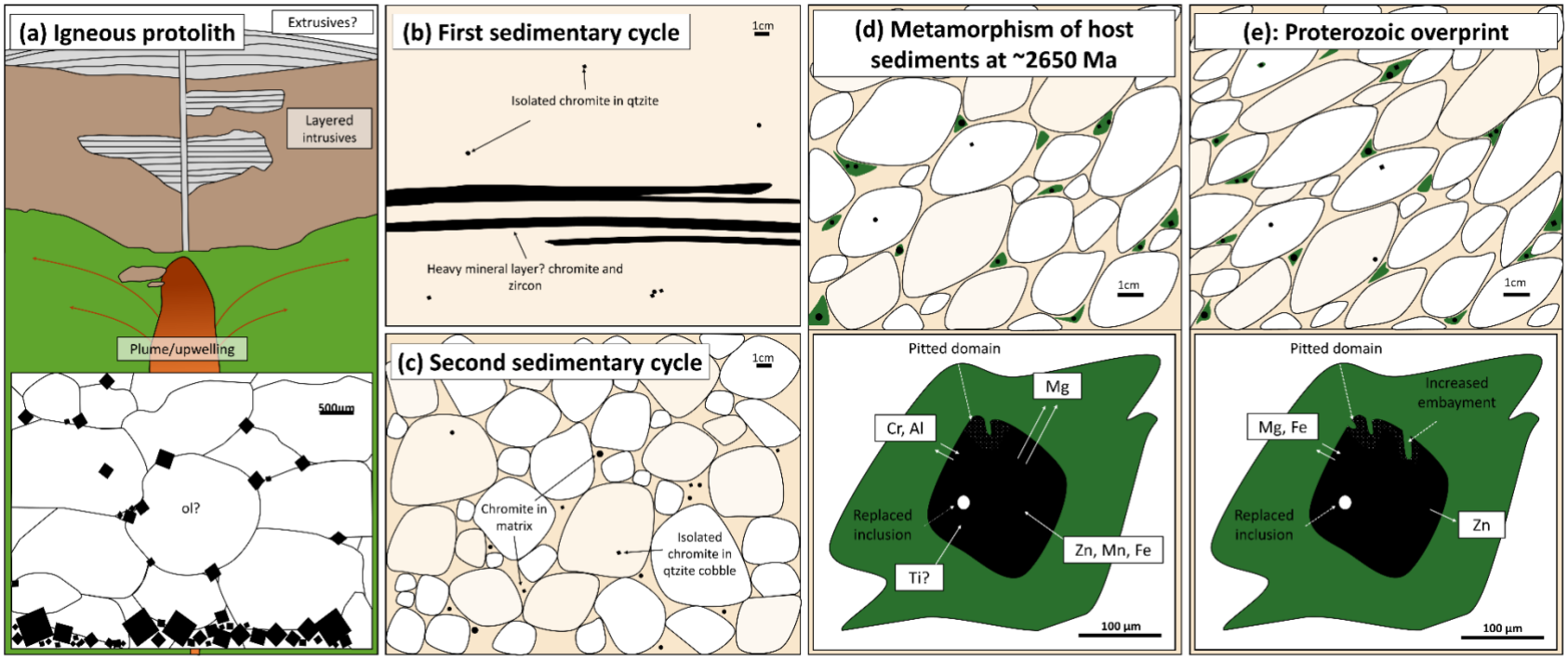
(a) Igneous protolith
Extrusives?
Layered intrusives
Plume/upwelling
500µm
ol?
(b) First sedimentary cycle
1cm
Isolated chromite in qtzite
Heavy mineral layer? chromite and zircon
(c) Second sedimentary cycle
1cm
Chromite in matrix
Isolated chromite in qtzite cobble
(d) Metamorphism of host sediments at ~2650 Ma
1cm
Pitted domain
Mg
Cr, Al
Replaced inclusion
Zn, Mn, Fe
Ti?
100 µm
(e): Proterozoic overprint
1cm
Pitted domain
Increased embayment
Mg, Fe
Replaced inclusion
Zn
100 µm

Fig. 15

Table 1: Representative EPMA analysis of Jack Hills chromites.													
Sample	**14WA1**	**14WA2**	**14WA3**	**14WA4**	**16WA5**	**16WA6**	**16WA7**	**16WA8**	**16WA9**	**16WA10**	**01JH35**	**01JH36**	**01JH54**
Grid Ref. (UTM)	499135E 7105846N	499135E 7105846N	499135E 7105846N	499135E 7105846N	499135E 7105846N	499141E 7105855N	499102E 7105837N	499096E 7105837N	499395E 7106007N	499393E 7106004N		499947E 7106431N	499137E 7105849N
Grain #	**4**	**17**	**44**	**28**	**19**	**12**	**7**	**5 core**	**2**	**20**	**4**	**5**	**5**
Rounding	RO	RO (2)	RO	RO/RC	RO	EO	RO/EO	RO/RC	EO	RC			
SiO_2	0.02	0.08	0.00	0.00	0.01	0.01	0.00	0.01	0.03	0.03	0.03	0.01	0.03
TiO_2	0.18	0.32	0.27	0.09	0.12	0.19	0.28	0.08	0.22	0.04	0.54	0.08	0.11
Al_2O_3	18.52	11.89	18.13	18.53	20.28	18.26	22.43	19.02	19.48	20.35	21.16	21.14	19.86
Cr_2O3	46.20	51.52	42.43	44.42	44.18	45.82	38.52	44.69	45.26	44.11	39.79	43.14	44.59
V_2O_3	0.12	0.19	0.16	0.11	n/a	n/a	n/a	n/a	0.14	0.13	0.23	0.12	0.14
Fe_2O_3	0.00*	3.97*	4.37*	0.82*	0.00*	0.00*	1.81*	0.05*	0.00*	0.00*	16.82¥	12.26¥	15.89¥
FeO	27.66	28.26	24.39	26.17	28.76	27.50	23.79	28.63	29.19	26.65	13.52	14.15	13.49
MgO	1.20	2.40	1.39	0.62	2.18	1.67	0.49	0.91	0.76	0.42	1.06	1.32	1.92
MnO	2.13	1.46	2.03	1.84	0.71	0.33	0.73	0.95	1.80	1.28	3.66	1.51	1.46
CaO	0.00	0.01	0.00	0.01	0.00	0.01	0.01	0.00	0.00	0.00	n/a	n/a	n/a
Na_2O	0.00	0.10	0.00	0.00	n/a	n/a	n/a	n/a	n/a	n/a	n/a	n/a	n/a
NiO	0.00	0.00	0.00	0.01	0.02	0.00	0.00	0.01	0.00	0.00	0.01	0.00	0.00
ZnO	3.08	0.84	7.29	6.19	2.11	4.32	11.24	3.95	1.39	5.50	2.22	4.74	1.80
CuO	n/a	n/a	n/a	n/a	n/a	n/a	n/a	n/a	n/a	n/a	0.01	0.02	0.00
Total	**99.10**	**101.03**	**100.46**	**98.80**	**98.38**	**98.11**	**99.31**	**98.31**	**98.27**	**98.52**	**99.05**	**98.87**	**99.29**
Mg#	7.20	11.83	8.03	3.95	11.90	9.77	3.30	5.36	4.44	2.76	12.19	14.24	20.24
Cr#	62.60	74.41	61.09	61.66	59.37	62.74	53.53	61.19	60.92	59.25	60.04	57.78	60.10
$Fe^{3+}/\Sigma Fe$	0.00	11.22	13.87	2.74	0.00	0.00	6.42	0.00	0.00	0.00	52.81	44.51	51.46
$Fe^{3+}/\Sigma R^{3+}$	0.00	5.17	5.65	1.07	0.00	0.00	2.34	0.00	0.00	0.00	18.32	13.86	16.93

Table 1: Representative EPMA analysis of chromite from each sample location. V_2O_3 not measured for 16WA5-7 and partial 16WA8. *Fe_2O_3 calculated from AB_2O_3 stoichiometry using the equations of Droop (1987). ¥Fe_2O_3 calculated by charge balance from direct EPMA measurement of oxygen.

Table 2: Oxygen isotopic composition ($\delta^{18}O_{VSMOW}$) of Jack Hills detrital chromites.						
Size fraction (μm)	105-149	149-210	210-300	300-350	350-425	Uncertainty (2sd)
01JH36	0.65		1.15	1.16		0.08
01JH36	0.73		1.41	1.71		
01JH36			1.41	1.77		
01JH36 Average	**0.69**		**1.32**	**1.55**		
01JH54		1.62	2.17	1.02	1.65	0.06
01JH54		1.69	2.2	1.17	2.11	
01JH54		2.07				
01JH54 Average		**1.79**	**2.19**	**1.10**	**1.88**	

Table 2: Oxygen isotopic composition ($\delta^{18}O_{SMOW}$) of detrital chromites from 01JH36 and 01JH54 determined by laser fluorination. Values represent deviation from standard mean ocean water (V-SMOW) in per mil (‰). Each analysis consisted of a ~2 mg aliquot of chromite separated by grain size.

Any separation by rounding shape?

Table 3: Representative EPMA compositions of 13TKN22 chromites and 16WA13 relict chromite cores.						
Sample	**13TKN22**	**13TKN22**	**13TKN22**	**16WA13**	**16WA13**	**16WA13**
Grid Ref. (UTM)				**489515E 7102336E**	**489515E 7102336E**	**489515E 7102336E**
Crystal #	**40**	**42**	**47**			
Classification	**chromite**	**chromite**	**chromite**	**relict chromite**	**relict chromite**	**relict chromite**
SiO_2	0.00	0.00	0.02	0.03	0.02	0.03
TiO_2	1.13	1.03	0.97	0.62	0.92	0.86
Al_2O_3	9.23	9.26	9.18	13.31	12.80	12.52
Cr_2O3	43.66	44.18	43.87	45.96	46.48	46.77
V_2O_3	n/a	n/a	0.25	n/a	n/a	n/a
Fe_2O_3	12.88	12.63	12.95	6.47	5.76	5.87
FeO	28.10	27.72	27.20	27.89	28.25	28.17
MgO	2.72	3.41	3.72	2.83	2.68	2.65
MnO	1.32	0.45	0.43	1.21	1.20	1.19
CaO	0.01	0.03	0.03	0.01	0.00	0.03
NiO	0.14	0.12	0.13	0.08	0.12	0.10
ZnO	0.60	0.59	0.58	1.08	1.06	1.08
Total	**99.80**	**99.43**	**99.33**	**99.10**	**99.61**	**99.30**
Mg #	14.73	17.99	14.59	13.00	12.49	12.37
Cr #	76.03	76.20	76.22	69.84	70.89	71.47
$Fe^{3+}/\Sigma Fe$	29.20	29.08	30.00	17.28	15.51	15.78
$Fe^{3+}/\Sigma R^{3+}$	17.59	17.18	17.64	8.56	7.72	7.86

Table 3: Representative EPMA analysis of chromite from Manfred Complex metaperidotite 13TKN22 and Jack Hills recrystallised ultramafic 16WA13. V_2O_3 not measured for some chromites within 13TKN22. Fe_2O_3 calculated from AB_2O_3 stoichiometry using the equations of Droop (1987).